# Main Manuscript for

## Intestinal microbiota modulates adrenomedullary response through Nod1 sensing in chromaffin cells

Chen Xiang[1, 2, #], Peihua Chen[3, #], Qin Zhang[1], Yinghui Li[1, 2], Ying Pan[1], Wenchun Xie[1, 4], Jianyuan Sun [3, *], Zhihua Liu [1, 5, 6, *]

1. Key Laboratory of Infection and Immunity, Institute of Biophysics, Chinese Academy of Sciences, Beijing 100101, China

2. University of Chinese Academy of Sciences, Beijing 100049, China

3. The Brain Cognition and Brain Disease Institute, Shenzhen Institutes of Advanced Technology, CAS; Shenzhen-Hong Kong Institute of Brain Science-Shenzhen Fundamental Research Institutions, Shenzhen, 518055, China

4. Guangdong Bio-healhtech Advanced Co., Ltd., Foshan 528000, China

5. Institute of Immunology, School of Medicine, Tsinghua University

6. Tsinghua-Peking Center for Life Sciences, 100084

[#]These authors contributed equally: Chen Xiang and Peihua Chen

*Corresponding authors

To whom correspondence may be addressed. Email: zhihualiu@ibp.ac.cn. or jy.sun1@siat.ac.cn.

ORCIDs: 0000-0002-0269-0901 Zhihua Liu; 0000-0002-1072-6230 Chen Xiang

## Keywords

Host-microbe crosstalk; Nod1; intracellular membrane trafficking

21 **Abstract**

22 The intestinal microbiota closely interacts with the neuroendocrine system and exerts profound

23 effects on host physiology. Many of the molecular mechanisms underlying these interactions await

24 discovery. Here we report that Nod1 ligand derived from intestinal bacteria directly modulates

25 catecholamine storage and secretion in mouse adrenal chromaffin cells. The cytosolic

26 peptidoglycan receptor Nod1 is involved in chromogranin A (CHGA) retention in dense core

27 granules (DCGs) in chromaffin cells in a cell-autonomous manner. Mechanistically, upon

28 recognizing its cognate ligands, Nod1 localizes to DCGs, and recruits Rab2a, which is critical for

29 CHGA retention in DCGs. Loss of Nod1 ligands leads to a profound defect in epinephrine storage

30 in chromaffin cells, and subsequently, less secretion upon stimulation. The intestine-adrenal

31 medulla crosstalk bridged by Nod1 ligands modulates adrenal medullary responses during the

32 immobilization-induced stress response in mice. Thus, our study uncovers a mechanism by which

33 intestinal microbes directly modulate a major pathway in response to stress, which may provide

34 further understanding of the gut-brain axis.

35 **Main Text**

36 **Introduction**

37 Accumulating evidence has shown that microbes residing in the intestine are deeply intertwined

38 with diverse aspects of host physiology, ranging from metabolism, immune system development

39 and immune responses, to neuronal development and activity (*Blander, Longman, Iliev,*

40 *Sonnenberg, & Artis, 2017; Fung, Olson, & Hsiao, 2017; Nicholson et al., 2012; Rooks & Garrett,*

41 *2016*). It is emerging that the neuroendocrine system closely interacts with the gut microbiota (*Farzi,*

42 *Frohlich, & Holzer, 2018*). Gut dysbiosis leads to profound alterations in neuroendocrine,

43 neurochemical and behavioral parameters (*Crumeyrolle-Arias et al., 2014; Foster & McVey Neufeld,*

44 *2013; Rogers et al., 2016; Zheng et al., 2016*). Conversely, neuroendocrine can play a significant

45 role in the gastrointestinal physiology, and malfunctioning neuroendocrine contributes to the

46 pathogenesis of gastrointestinal disorders, including inflammatory bowel diseases (*Brinkman, Ten*

47 *Hove, Vervoordeldonk, Luyer, & de Jonge, 2019; El-Salhy, Solomon, Hausken, Gilja, & Hatlebakk,*

48 *2017*). Uncovering the molecular mechanisms underlying such crosstalk between microbes and

49 the neuroendocrine system is of importance to understand the role of the microbiota in host health

50 and disease.

51 The neuroendocrine system controls vital processes in response to acute or chronic stress,

52 which has been critical for host survival during the long history of evolution. The sympatho-adrenal-

53 medullary (SAM) and hypothalamic-pituitary-adrenocortical (HPA) axes are the primary systems

54 involved in the stress response. The SAM axis was first described by Cannon and colleagues to be

55 involved in acute stress response, generally known as the "fight-or-flight" response (*Cannon, 1914*).

56 The acute stress response involves increased circulating levels of adrenaline (primarily from the

57 adrenal medulla) and noradrenaline (primarily from sympathetic nerves), increased heart rate and

58 force of contraction, peripheral vasoconstriction, and energy mobilization (*Tank & Lee Wong, 2015*).

59 For the HPA axis, stressors lead to secretion of corticotropin-releasing hormone (CRH) from the

60 paraventricular nucleus (PVN) of the hypothalamus, and CRH acts on the pituitary gland, resulting

61 in release of adrenocorticotrophic hormone (ACTH), which in turn cause the adrenal cortex to

62    release the stress hormone cortisol (*Tsigos & Chrousos, 2002*). The HPA axis and the sympathetic

63    system act in a complementary manner throughout the body during stress. Cortisol, together with

64    epinephrine and norepinephrine, prepares the body for the stress response, which is characterized

65    by gluconeogenesis, increased blood sugar, body temperature change, decreased immune

66    function, and increased metabolism of fat and protein (*Khani & Tayek, 2001; Padgett & Glaser,*

67    *2003; Ste Marie & Palmiter, 2003; Tank & Lee Wong, 2015*).

68         It is interesting to know whether the intestinal microbiota may impact stress responses. Indeed,

69    the effect of microbiota on HPA axis activation has been extensively examined. Absence of

70    microbiota (germ-free status) in rodents leads to exaggerated activation of the HPA axis associated

71    with elevated ACTH and corticosterone levels in response to stress, accompanied with anti-anxiety

72    and anti-depression behavior changes (*Diaz Heijtz et al., 2011; Huo et al., 2017; Sudo et al., 2004;*

73    *Zheng et al., 2016*). Of note, it is also reported that such behavior changes may depend on genetic

74    background and husbandry (*Farzi et al., 2018*). Mechanistically, it has been shown that the

75    microbiota regulates the expression of critical HPA axis genes both directly and indirectly (*Farzi et*

76    *al., 2015; Luo et al., 2018; Shanks, Larocque, & Meaney, 1995*). One of the mechanisms may

77    involve innate immune receptors, such as Toll-like receptors (TLRs). For instance, acute TLR4

78    activation triggers the HPA axis, likely through the action of cytokines (*Liu, Buisman-Pijlman, &*

79    *Hutchinson, 2014; Zacharowski et al., 2006*). TLR2-deficient mice also exhibit impaired adrenal

80    corticosterone release after inflammatory stress induced by bacterial cell wall compounds

81    (*Bornstein et al., 2004*). In comparison, the effect of intestinal microbiota on the SAM pathway has

82    not been extensively investigated. One previous finding found that the absence of gut microbial

83    colonization selectively impaired catecholamine response to hypoglycemic stress in mice.(*Giri, Hu,*

84    *La Gamma, & Nankova, 2019*)

85         In the SAM pathway, upon stimulation from sympathetic nerves, adrenal chromaffin cells

86    located in the adrenal medulla secrete catecholamines (mainly epinephrine), which are the

87    hormones necessary in the fight-or-flight response (*Eisenhofer, Kopin, & Goldstein, 2004*). Adrenal

88    chromaffin cells convert tyrosine to catecholamines in a complex multi-step process (*Berends et*

89    *al., 2019*). The catecholamines are then stored and bound to chromogranin A (CHGA) in dense

90    core granules (DCGs) (*Jirout et al., 2010; Mahapatra et al., 2004; Videen, Mezger, Chang, &*

91    *O'Connor, 1992*). CHGA is involved in DCG biogenesis by preventing degradation of granule

92    proteins and packing synthetic catecholamines in DCGs (*Kim, Zhang, Sun, Wu, & Loh, 2005*).

93    CHGA deficiency led to a 30-40% reduction in catecholamine secretion from adrenal chromaffin

94    cells in mice (*Pasqua et al., 2016*). Similarly, knockdown of CHGA in PC-12 cells, a neuroendocrine

95    cell line, decreased the number of DCGs and impaired DCG formation (*Kim, Tao-Cheng, Eiden, &*

96    *Loh, 2001*). Thus, CHGA plays a key role in epinephrine storage in chromaffin cells.

97    Nucleotide-binding oligomerization domain 1 (Nod1), together with Nod2, as classic pattern

98    recognition receptors (PRRs), play a key role in innate immunity responses by recognizing

99    conserved microbial molecules from invading pathogens (*Chamaillard et al., 2003; Mogensen,*

100   *2009*). Studies have found that Nod1 and Nod2 are involved in mediating the gut-brain crosstalk.

101   Mice deficient in both Nod1 and Nod2 (NodDKO) exhibited elevated anxiety levels in the context of

102   a hyperactive HPA axis (*Schneider, Zhang, Barrett, & Gareau, 2016*). Specific deletion of Nod1 in

103   intestinal epithelium resulted in altered gastrophysiology and 5-hydroxytryptamine (5-HT) signaling,

104   which was speculated to be responsible for the altered behaviors in NodDKO mice following

105   exposure to stress (*Pusceddu et al., 2019*).

106   While it is traditionally thought that Nod proteins are cytosolic peptidoglycan (PGN) sensors

107   without recognizable membrane-targeting domains (*Inohara & Nunez, 2003*), several studies have

108   found that Nod1 and Nod2 can be recruited to the plasma membrane and the membranes of

109   endosomes and DCGs (*Bonham & Kagan, 2014; Lu et al., 2019; Travassos et al., 2010; Zhang et*

110   *al., 2015; Zhang et al., 2019*). Membrane localization of Nod1 and Nod2 has been found to be vital

111   for their function. For example, plasma membrane localization of Nod1 and Nod2 is critical for NF-

112   kB activation in macrophages (*Lu et al., 2019; Nakamura et al., 2014*). Nod1 and Nod2 recruit

113   ATG16L1 onto the plasma membrane to initiate autophagy of bacteria entering the host cell

114   (*Cadwell, 2016; Travassos et al., 2010*). Nod1 and Nod2 are both implicated in processing bacterial

115   outer membrane vesicles through early endosome or autophagosome pathways (*Chu et al., 2016;*

116     *Travassos et al., 2010*). We previously reported that DCG-localized Nod1 regulates an intracellular

117     membrane trafficking event to promote insulin secretion in pancreatic beta cells (*Zhang et al., 2019*).

118     Therefore, membrane localization of Nod proteins may be essential for fulfilling their diverse

119     functions in different cell contexts.

120     In this study, we found that Nod1 was highly expressed in adrenal chromaffin cells. We probed

121     for the effect of intestinal microbe-derived Nod1 ligands on hormone secretion in chromaffin cells.

122     Mechanistically, we found that Nod1 localized to DCGs and recruited Rab2a onto DCGs, which

123     subsequently affects CHGA retention in DCGs. Microbe-sensing through Nod1 is required for

124     efficient storage and secretion of catecholamines in adrenal chromaffin cells. Finally, specific

125     deficiency of Nod1 in chromaffin cells impairs epinephrine secretion during immobilization stress in

126     mice. Collectively, our results identify a new microbe-host crosstalk pathway, in which adrenal

127     chromaffin cells directly sense microbial Nod1 ligands released from commensal bacteria by

128     intestinal lysozyme to optimize epinephrine secretion during immobilization stress.

129     **Results**

130     **Nod1 affects CHGA and epinephrine abundance in adrenal chromaffin cells in a cell-**

131     **autonomous manner.**

132     Immunohistochemical staining in WT mice detected Nod1 expression specifically in the adrenal

133     medulla, but not in the cortex region, while *Nod1* deficiency abolished the medullary staining (*Figure*

134     *1A*). In the adrenal gland, *Nod1* mRNA was highly enriched in medulla compared to cortex (*Figure*

135     *1—figure supplement 1A*). The medullary *Nod1* mRNA level was comparable to that in spleen,

136     which is known to express Nod1 at a high level (*Figure 1B*), as previously reported (*Inohara et al.,*

137     *1999*).

138     We next sought to understand the biological function of Nod1 in adrenal chromaffin cells.

139     Adrenal chromaffin cells are classic neuroendocrine cells, with DCGs as the hallmark.

140     Transmission electron microscopy (TEM) analysis showed the classic dense core morphology of

141     DCGs in WT chromaffin cells, while a significant portion of DCGs in *Nod1$^{-/-}$* chromaffin cells did

142   not have the typical dense core (*Figure 1C-D*). The diameters of dense cores in *Nod1$^{-/-}$* chromaffin

143   cells tended to be smaller than those in WT chromaffin cells (*Figure 1E*). These data indicate that

144   *Nod1* deficiency led to abnormalities in DCG formation in chromaffin cells.

145        CHGA plays a key role in the formation of the dense core in DCGs. We probed for CHGA in

146   adrenal medullas of WT and *Nod1$^{-/-}$* mice and found that the CHGA staining signal was significantly

147   reduced in *Nod1$^{-/-}$* medullas compared to WT medullas (*Figure 1F*). Staining of synaptophysin and

148   phogrin, two membrane markers of DCGs, was comparable between WT and *Nod1$^{-/-}$* mice (*Figure*

149   *1F* and *Figure 1—figure supplement 1B*). Immunoblotting showed a significantly reduced CHGA

150   protein level in isolated adrenal medullas from *Nod1$^{-/-}$* mice compared to WT mice (*Figure 1G-H*),

151   which confirms our immunofluorescence staining data on tissue sections. *CHGA* mRNA levels were

152   comparable in WT and *Nod1$^{-/-}$* chromaffin cells (*Figure 1—figure supplement 1C*). CHGA is critical

153   for packaging epinephrine in chromaffin cells (*Pasqua et al., 2016*). We used an antibody to probe

154   for epinephrine in adrenal medullas and found that the fluorescence signal of the anti-epinephrine

155   antibody was weaker in medullas from *Nod1$^{-/-}$* mice compared to medullas from WT mice (*Figure*

156   *1I*). Tyrosine hydroxylase (TH) was stained to label chromaffin cells (*Figure 1I*). We further

157   quantified the amount of epinephrine in adrenal glands and found that *Nod1* deficiency markedly

158   reduced the abundance of epinephrine (*Figure 1J*).

159        We wondered whether Nod1 might be involved in affecting the abundance of CHGA and

160   epinephrine in a cell-autonomous manner. To test this possibility, we specifically deleted Nod1 in

161   adrenergic and noradrenergic cells by generating *Dbh-cre;Nod1$^{f/f}$* mice, in which loxP-flanked *Nod1*

162   alleles (*Nod1$^{f/f}$*) were deleted by Cre recombinase driven by the dopamine beta hydroxylase (Dbh)

163   promoter). In *Dbh-cre;Nod1$^{f/f}$* mice, the *Nod1* mRNA level was markedly reduced in adrenal gland,

164   but not in other tissues, such as spleen or lung (*Figure 1—figure supplement 1D*). Specific deletion

165   of Nod1 in chromaffin cells led to marked reduction in staining of epinephrine and CHGA (*Figure*

166   *1K*). Accordingly, adrenal glands from *Dbh-cre;Nod1$^{f/f}$* mice contained less epinephrine than control

167   *Nod1$^{f/f}$* mice (*Figure 1L*). Thus, deficiency of Nod1 led to reduced levels of CHGA and epinephrine

168   in DCGs in a cell-autonomous manner.

169 **Microbial Nod1 ligand regulates the amount of CHGA and epinephrine in DCGs.**

170 Nod1 is a cytosolic receptor which has been implicated in recognizing peptidoglycan ligands from

171 pathogens as well as intestinal commensals (*Chamaillard et al., 2003*). We suspected that Nod1

172 ligand from intestinal microbes might be involved in regulating Nod1 in adrenal chromaffin cells.

173 Treatment with antibiotics has been used to deplete microbial ligands in the circulation (*Arentsen*

174 *et al., 2017; Bird, 2010; Clarke et al., 2010; Hergott et al., 2016*). We previously reported that the

175 presence of circulating Nod1 ligand depends on lysozyme in the intestinal lumen, and deficiency of

176 Lyz1 in mice leads to depletion of microbial Nod1 ligands (*Zhang et al., 2019*). To determine the

177 effect of intestinal Nod1 ligand on Nod1 in chromaffin cells, we used mice treated a cocktail of

178 antibiotics (ABX) and $Lyz1^{-/-}$ mice. We compared Nod1 staining in WT mice, ABX mice and $Lyz1^{-/-}$

179 mice. We found that Nod1 localized to $CHGA^+$ DCGs in specific pathogen-free (SPF) WT mice, but

180 the staining of Nod1 on $CHGA^+$ DCGs was very weak in germ-free (GF) mice, which lack gut

181 microbiota (*Figure 2A*). Depletion of commensal bacteria by antibiotic cocktail treatment or

182 depletion of Lyz1 diminished the staining of Nod1 on $CHGA^+$ DCGs (*Figure 2A*). mRNA

183 quantification and IHC of adrenal medullas showed that ABX treatment or loss of Lyz1 did not affect

184 the protein expression of Nod1 (*Figure 2—figure supplement 1A-B*). This indicates that the

185 diminished staining of Nod1 in chromaffin cells in ABX or $Lyz1^{-/-}$ mice was due to reduced

186 recruitment of Nod1 onto DCGs.

187 Similar to the observation in $Nod1^{-/-}$ mice, CHGA staining was greatly diminished in ABX or

188 $Lyz1^{-/-}$ mice (*Figure 2A* and *Figure 2—figure supplement 1C*). In comparison, localization of Nod1

189 on Golgi was not affected in ABX mice or $Lyz1^{-/-}$ mice compared to WT mice (*Figure 2—figure*

190 *supplement 1D*). Significantly less CHGA was detected in isolated adrenal glands of $Lyz1^{-/-}$ mice

191 compared to WT mice (*Figure 2B*). Immunofluorescence staining detected marked reduction of

192 epinephrine in $TH^+$ cells in adrenal gland in ABX mice or $Lyz1^{-/-}$ mice compared to WT mice (*Figure*

193 *2C*). Accordingly, the levels of epinephrine and CHGA were both reduced in adrenal gland in ABX

194 mice and $Lyz1^{-/-}$ mice compared to WT mice (*Figure 2—figure supplement 1E*). The reduction in

195　epinephrine in adrenal gland in ABX mice and *Lyz1$^{-/-}$* mice was confirmed by ELISA quantification

196　(*Figure 2D-E*). Furthermore, the reduction in CHGA in chromaffin cells from *Lyz1$^{-/-}$* mice was

197　observed in cultured primary chromaffin cells, and treatment with the cognate Nod1 ligand, iE-DAP,

198　restored CHGA in chromaffin cells from *Lyz1$^{-/-}$* mice (*Figure 2F*). This indicates that Nod1 ligand is

199　required to maintain the CHGA level in chromaffin cells.

200　**Nod1 recruits Rab2a onto DCGs to regulate CHGA retention in DCGs.**

201　Rabs, a family of small GTPases, are master regulators of intracellular membrane trafficking.

202　Rab2a is known to be a Golgi-resident GTPase, governing intra-Golgi trafficking (*Ailion et al., 2014;*

203　*Buffa, Fuchs, Pietropaolo, Barr, & Solimena, 2008*). In addition, Rab2a localizes to the membranes

204　of lysosome-like organelles, such as DCGs, melanosomes and early endosomes. Studies have

205　shown that Rab2a regulates cargo sorting events in neurons in *C. elegans* and intestinal Paneth

206　cells (*Edwards et al., 2009; Sumakovic et al., 2009; Zhang et al., 2015*). In *C. elegans*, Rab2 null

207　mutation impaired the maturation of the dense core of DCGs, and DCG cargos were mistrafficked

208　to early endosomes for degradation (*Edwards et al., 2009; Sumakovic et al., 2009*). In intestinal

209　Paneth cells, Rab2a knockdown led to mistargeting of lysozyme to lysosomes for degradation

210　instead of storage in DCGs (*Zhang et al., 2015*). Thus, we suspected that Rab2a might act

211　downstream of Nod1 in regulating CHGA storage in DCGs. We performed immunostaining of

212　Rab2a and Nod1 in adrenal medulla. Rab2a and Nod1 largely colocalized in WT chromaffin cells;

213　however, colocalization of Rab2a and Nod1 was largely lost in chromaffin cells from ABX or *Lyz1$^{-/-}$*

214　mice (*Figure 3A*). In contrast, the colocalization of Rab2a with Nod1 around the nucleus was not

215　affected in chromaffin cells from ABX or *Lyz1$^{-/-}$* mice (*Figure 3A*). Nod1 localizes to DCGs and the

216　perinuclear Golgi (*Figure 2A* and *Figure 2—figure supplement 1D*); therefore, we suspect that the

217　remaining colocalization of Nod1 and Rab2a in the perinuclear region was Golgi localization, which

218　remained undisturbed in chromaffin cells from ABX or *Lyz1$^{-/-}$* mice. To test that possibility that

219　Nod1 specifcially affects Rab2a localization onto DCGs, we performed immunostaining of Rab2a

220　together with GM130, a Gogli marker. We found that, in addition to localizing to Golgi marked by

9

221   GM130, Rab2a staining was also observed on puncta throughout in the cytosol in the control *Nod1*^f/f

222   mice (*Figure 3B*). However, specific depletion of Nod1 in chromaffin cells in *Dbh-cre;Nod1*^f/f mice

223   resulted in the loss of Rab2a staining on puncta in the cytosol (*Figure 3B*). In comparison, the

224   localization of Rab2a on Gogli was not affected in chromaffin cells in *Dbh-cre;Nod1*^f/f mice (*Figure*

225   *3B*).

226       To determine whether Rab2a affects CHGA retention in DCGs, we determined the effect of

227   Rab2a on CHGA in PC-12 cells, derived from a pheochromocytoma of the rat adrenal medulla

228   (*Greene & Tischler, 1976*). To perturb the activity of Rab2a, we created a Rab2a mutant, S20N,

229   which was previously determined as a dominant negative mutant (*Tisdale, Bourne, Khosravi-Far,*

230   *Der, & Balch, 1992*). Expression of Rab2a-WT did not alter the level of CHGA in transfected cells;

231   however, expression of the S20N mutant resulted in significant reduction of CHGA (*Figure 3C-D*).

232   It was previously shown that loss of Rab2a mistargeted DCG cargos for degradation in lysosomes

233   (*Edwards et al., 2009; Sumakovic et al., 2009; Zhang et al., 2015*). We treated PC-12 cells

234   expressing Rab2a S20N with a lysosome inhibitor, leupeptin. The leupeptin treatment effectively

235   restored CHGA in cells expressing the Rab2a S20N mutant (*Figure 3C-D*). Thus, Rab2a activity is

236   involved in regulating the level of CHGA in DCGs.


237   **Reduced catecholamine secretion in chromaffin cells deficient in Nod1 or Nod1 ligand.**

238   We next decided to determine whether reduced storage of CHGA and epinephrine could lead to

239   reduced hormone secretion. Single-cell amperometry measures the numbers of released

240   catecholamine molecules during every individual exocytosis event (*Garcia, Garcia-De-Diego,*

241   *Gandia, Borges, & Garcia-Sancho, 2006; Wightman et al., 1991*). Basically, catecholamines from

242   each vesicle are captured and oxidized on a carbon electrode, resulting in a current (or

243   amperometric) peak for each vesicle that bursts (*Figure 4A*). Each validated current peak presents

244   a fusion event, and the number of catecholamine molecule from each fusion event is calculated

245   from the integration of each single current event (*Garcia et al., 2006; Wightman et al., 1991*). Single-

246   cell amperometry does not distinguish different kinds of catecholamines, but it can accurately

247  quantify the number of molecules released and the kinetic parameters of each vesicle (*Dunevall et*

248  *al., 2015*). Single-cell amperometry was employed to record each K$^+$-stimulated fusion event

249  between secretory vesicles and the plasma membrane on cultured primary chromaffin cells from

250  WT, *Nod1$^{-/-}$* and *Lyz1$^{-/-}$* mice (*Figure 4B*). The peak current of individual amperometric spike

251  events was distributed toward reduced current in *Nod1$^{-/-}$* and *Lyz1$^{-/-}$* chromaffin cells (*Figure 4C*),

252  and the means of peak current were reduced in *Nod1$^{-/-}$* and *Lyz1$^{-/-}$* chromaffin cells compared with

253  WT cells (*Figure 4D*). The catecholamine molecule numbers from each fusion event was calculated.

254  The distribution of catecholamine molecule numbers, together with the mean numbers of secreted

255  catecholamine molecules per event, indicated that fewer catecholamine molecules were secreted

256  from *Nod1$^{-/-}$* and *Lyz1$^{-/-}$* chromaffin cells compared with WT cells (*Figure 4E-F*). Taken together,

257  these data indicate that the deficiency of Nod1 or Lyz1 leads to impaired catecholamine secretion

258  in DCGs.

259  Single-cell amperometry does not distinguish epinephrine and norepinephrine from other

260  monoamines, including dopamine (*Robinson, Venton, Heien, & Wightman, 2003*). Specific probes

261  have been developed to monitor catecholamine dynamics in a real-time manner (*Muller, Joseph,*

262  *Slesinger, & Kleinfeld, 2014; Wang, Jing, & Li, 2018*). A GPCR activation-based NE (GRAB$_{NE}$)

263  sensor, based on an α-2 adrenergic receptor, has been used for *in vivo* and *in vitro* measurement

264  of epinephrine or norepinephrine dynamics in mice (*Feng et al., 2019*). The GRAB$_{NE}$ sensor has

265  circularly permutated eGFP (cp eGFP) inserted between the fifth and sixth transmembrane

266  domains of the α-2 adrenergic receptor. When epinephrine or norepinephrine binds to the

267  extracellular domain of the GRAB$_{NE}$ sensor, a conformational change occurs between the fifth and

268  sixth transmembrane domains to activate the green fluorescence of cp eGFP. Thus, when GRAB$_{NE}$

269  sensor is expressed on the cell surface, its fluorescence reflects the level of

270  epinephrine/norepinephrine in the extracellular environment (*Feng et al., 2019*). Adrenal chromaffin

271  cells mostly secrete epinephrine, so we employed the GRAB$_{NE}$ method to evaluate whether Nod1

272  or Nod1 ligand could affect the secretion of epinephrine (and, to a lesser extent, norepinephrine).

273  Chromaffin cells from WT, *Nod1$^{-/-}$* or *Lyz1$^{-/-}$* mice were isolated and transfected with GRAB$_{NE}$

274  sensor. As control, RFP was co-transfected to provide continuous fluorescence in the cytoplasm,

275  as previously described (*Feng et al., 2019*). The green fluorescence on the plasma membrane in

276  WT cells increased rapidly when cells were exposed to a high concentration of $K^+$, and then

277  gradually decreased and returned to the ground state as time elapsed (*Figure 5A*). RFP in the

278  cytoplasm remained constant during the course of $K^+$ stimulation (*Figure 5—figure supplement 1*).

279  In comparison, $K^+$ stimulation did not prompt a strong enhancement in the green fluorescence on

280  the plasma membrane of the transfected $Nod1^{-/-}$ or $Lyz1^{-/-}$ chromaffin cells (*Figure 5A*). The

281  fluorescence intensity changes of $GRAB_{NE}$ on the plasma membrane and of RFP were recorded

282  and quantified. Loss of *Nod1* or *Lyz1* in mice resulted in a weaker increase in the fluorescence

283  intensity of the $GRAB_{NE}$ sensor, compared to WT mice (*Figure 5B*). The maximum fluorescence

284  intensity change of $GRAB_{NE}$ was also reduced in chromaffin cells from $Nod1^{-/-}$ or $Lyz1^{-/-}$ mice,

285  compared to cells from WT mice (*Figure 5C*). These data indicate that less epinephrine

286  (norepinephrine) was secreted by cells from $Nod1^{-/-}$ or $Lyz1^{-/-}$ mice. We further supplemented

287  cultured primary chromaffin cells from $Lyz1^{-/-}$ mice with iE-DAP. Such treatment restored the $K^+$-

288  stimulated fluorescence augmentation of the $GRAB_{NE}$ sensor (*Figure 5B-C*), which indicates that

289  the absence of Nod1 ligand was responsible for the decreased secretion of epinephrine by cells

290  from $Lyz1^{-/-}$ mice. In addition, chromaffin cells isolated from $Dbh-cre;Nod1^{f/f}$ mice also displayed a

291  similar reduction in epinephrine (norepinephrine) secretion (*Figure 5D-F*), further supporting the

292  idea that Nod1 plays a cell-autonomous role in regulating secretion in chromaffin cells.

293  **Deficiency of Nod1 ligand impairs the stress response.**

294  We wanted to determine the physiological function of Nod1 sensing in adrenal chromaffin cells. We

295  employed a mouse immobilization model, which has been widely used to evaluate the adrenal

296  medullary response during stress. The elevated epinephrine, together with other stress hormones,

297  induces a range of physiological responses in preparation for the fight-or-flight response, including

298  increased blood sugar level, glycogen mobilization in the liver, *etc.* (*Buira et al., 2004; Fernandez*

299  *et al., 2000; Kang, Sim, Park, Sharma, & Suh, 2015; Park et al., 2016*). We performed the

12

300      immobilization with WT and *Lyz1*^{−/−} mice. WT and *Lyz1*^{−/−} mice had comparable levels of circulating

301      epinephrine under basal (non-stressed) conditions (*Figure 6A*). When the mice were immobilized

302      for one hour, the level of circulating epinephrine markedly increased in WT mice, but the increase

303      was blunted in *Lyz1*^{−/−} mice (*Figure 6A*). Prior studies have found that immobilization raises the

304      blood sugar level (*Kang et al., 2015; Park et al., 2016*). We found that the surge in blood sugar was

305      clearly detected in both *Lyz1*^{−/−} and WT mice after restraint (*Figure 6B*).

306          To further determine the cell-autonomous function of Nod1 in adrenal medulla, we evaluated

307      control and *Dbh-cre;Nod1*[f/f] mice under immobilization. Control and *Dbh-cre;Nod1*[f/f] mice had a

308      comparable level of circulating epinephrine (*Figure 6C*). Immobilization resulted in a dramatic

309      increase in the circulating epinephrine level in control mice, while the increase in epinephrine level

310      was less pronounced in *Dbh-cre;Nod1*[f/f] mice (*Figure 6C*). The increase in blood sugar was also

311      blunted in *Dbh-cre;Nod1*[f/f] mice compared to control mice (*Figure 6D*). Furthermore, the stressed-

312      induced depletion of glycogen store in liver in *Dbh-cre;Nod1*[f/f] mice was milder compared to control

313      mice (*Figure 6E*). Thus, our data demonstrate that Nod1 sensing in adrenal medulla is involved in

314      epinephrine secretion during immobilization stress.

315      **Discussion**

316      Here we report that commensal bacteria are sensed directly in adrenal chromaffin cells to modulate

317      epinephrine output during immobilization stress. Upon sensing its ligand, Nod1 recruits Rab2a onto

318      DCGs, which assists the condensation of CHGA in DCGs. Defects in this pathway lead to reduced

319      epinephrine secretion in mouse. Thus, our study unveils a physiological role of Nod1-mediated

320      crosstalk between intestine and adrenal medulla to promote the fight-or-flight response.

321          Our study investigated the effect of Nod1 on epinephrine secretion in the adrenal medullary

322      response. In our study, adrenal chromaffin cells expressed Nod1 at a high level, and depletion of

323      Nod1 in adrenal chromaffin cells led to a dramatic reduction in CHGA and epinephrine. The effects

324      on CHGA and epinephrine were observed in cultured primary chromaffin cells, thus supporting a

325      cell-autonomous role of Nod1 in chromaffin cells. Supplementing cultured primary chromaffin cells

326   from *Lyz1*$^{-/-}$ mice with Nod1 ligand *in vitro* restored epinephrine secretion, which argues for a direct

327   effect of microbial ligands on chromaffin cells. We employed conditional Nod1 knockout mice to

328   further establish the cell-autonomous role of Nod1 in chromaffin cells. In *Dbh-cre;Nod1*$^{f/f}$ mice,

329   Nod1 was depleted in adrenal chromaffin cells and Dbh-expressing (Dbh$^+$) neurons. Adrenal

330   chromaffin cells are the main source of epinephrine during stress (*Axelrod & Weinshilboum, 1972*).

331   We observed a major reduction in the level of circulating epinephrine in *Dbh-cre; Nod1*$^{f/f}$ mice

332   compared to control mice. Thus, we propose that Nod1 sensing in adrenal chromaffin cells

333   regulates epinephrine secretion and consequently plays a critical role in the stress response. Of

334   course, we cannot exclude the possibility that Nod1 may play roles in other catecholaminergic Dbh$^+$

335   neurons during the stress response. It remains to be determined whether Nod1 expressed in cells

336   other than intestinal epithelium and adrenal chromaffin cells may regulate other aspects of

337   physiological processes involved in the stress response.

338      We found that loss of microbial Nod1 ligand results in impaired storage and secretion of

339   epinephrine in DCGs. Mechanistically, we found that *Nod1*$^{-/-}$, *Lyz1*$^{-/-}$, and *Dbh-cre;Nod1*$^{f/f}$ mice

340   contained lower levels of CHGA and epinephrine. CHGA has been shown to regulate

341   catecholamine-containing dense-core chromaffin granule biogenesis in the adrenal gland (*Díaz-*

342   *Vera et al., 2012; Kim et al., 2001; Pasqua et al., 2016*). We attribute the reduced storage of

343   epinephrine to the reduced amount of CHGA. The previous finding found that the absence of gut

344   microbial colonization selectively impaired catecholamine response to hypoglycemic stress in mice,

345   and transcriptome in adrenal glands was altered (*Giri et al., 2019*). It is possible that Nod1 regulated

346   storage of epinephrine may also contribute to impaired catecholamine response to hypoglycemic

347   stress.

348      CHGA plays a key role in epinephrine storage. Our results found that mRNA levels of CHGA

349   was not affected while protein levels of CHGA were reduced in adrenal medullas in *Nod1*$^{-/-}$, *Lyz1*$^{-/-}$,

350   and *Dbh-cre;Nod1*$^{f/f}$ mice. Thus, we did not perform whole-genome transcriptome profiling, and

351   instead, we focused our investigation on membrane trafficking event of CHGA. We observed

352   reduced recruitment of Rab2a onto DCGs in *Nod1*$^{-/-}$, *Lyz1*$^{-/-}$, and *Dbh-cre;Nod1*$^{f/f}$ mice.

14

353  Overexpressing a dominant negative mutant of Rab2a reduced the level of CHGA in PC-12 cells,

354  which could be restored by inhibiting lysosomes. We propose a scenario where a reduced level of

355  Nod1 or Nod1 ligand impairs Rab2a recruitment onto DCG membranes, which may cause

356  mistargeting of a significant proportion of CHGA to lysosomes for degradation. The involvement of

357  Rab2a in DCG cargo sorting has been previously reported (*Edwards et al., 2009; Sugawara, Kano,*

358  *& Murata, 2014; Sumakovic et al., 2009; Zhang et al., 2015*). Loss of Rab2a in neurons in *C.*

359  *elegans* led to specific lysosomal degradation of a neuropeptide that is normally located in DCGs

360  (*Edwards et al., 2009; Sumakovic et al., 2009*). Knockdown of Rab2a led to lysosomal degradation

361  of lysozyme in intestinal Paneth cells (*Zhang et al., 2015*). Besides DCGs, Rab2a also functions at

362  various steps of intracellular membrane trafficking, including ER-Golgi transport, autophagy and

363  autolysosome formation, and endosome-lysosome fusion. Indeed, our results show that Nod1 also

364  localizes to the Golgi. However, Rab2a localization around the Golgi was not affected by loss of

365  Nod1. Therefore, by unknown mechanisms, Nod1 together with Nod1 ligand is required to recruit

366  Rab2a onto DCGs. We suspect some other factors downstream of Nod1 are involved in recruiting

367  Rab2a onto DCGs, which warrants further investigation.

368      It was previously reported that Nod1 together with Rip2 recruited Rab1a onto insulin granules

369  in islet beta cells to regulate an anterograde transport event (*Zhang et al., 2019*). We found no

370  difference in Rab1a localization on DCGs in chromaffin cells in WT and *Nod1*$^{-/-}$ mice (data not

371  shown). It is intriguing that Nod1 recruits different Rab proteins onto vesicles in different cell types.

372  Additional factors may be involved in recruiting specific downstream Rab proteins in different cell

373  types.

374      In summary, Nod1 ligand from intestinal microbes directly modulates the storage of CHGA and

375  epinephrine in DCGs in adrenal chromaffin cells, which optimizes epinephrine secretion under

376  stress conditions. Thus, our study further exemplifies Nod1 as a key signaling molecule in the

377  microbiota-intestine-brain axis.

378 **Experimental model and subject details**

379 **Mice**

380 *Lyz1$^{-/-}$*, *Nod1$^{-/-}$* and *Nod1$^{f/f}$* mice (C57BL/6 background) were generated using the CRISPR/Cas9

381 method as described previously (*Zhang et al., 2019*). The *Dbh-Cre* (Tg(Dbh-

382 cre)KH212Gsat/Mmucd) mice were a gift from Professor Chen Zhan (NIBS) and were originally

383 from the Mutant Mouse Resource & Research Center (MMRRC) (*Gerfen, Paletzki, & Heintz, 2013*).

384 The *Dbh-cre* mice were further crossed with *Nod1$^{f/f}$* to generate conditional knockout (*Dbh-*

385 *cre;Nod1$^{f/f}$*) mice. 2-4-month-old gender-matched mice (both male and female) were used in this

386 study unless noted otherwise. All mice were bred at 3-6 animals per cage in a 12/12 h light-dark

387 cycle with *ad libitum* access to food and water at a controlled temperature (23°C ± 2°C). All specific

388 pathogen-free (SPF) mice were bred and housed in an AAALAC-accredited barrier facility in

389 Tsinghua University. All procedures were approved by the Committee of Institutional Animal Care

390 and Research, Tsinghua University.

391 **Method details**

392 **Plasmids**

393 Human Rab2a cDNA was reverse-transcribed from mRNA prepared from HEK293T cells and

394 inserted into peGFP-C1 vector. The dominant-negative (S20N) Rab2a mutant was generated by

395 PCR-mediated mutagenesis. Sequences were confirmed by Sanger sequencing.

396 **Cell culture and immunofluorescence**

397 PC-12 cells were cultured in RPMI-1640 medium supplemented with 10% fetal bovine serum and

398 1% Pen/Strep. The cells were cultured at 37°C in a humidified atmosphere containing 5% $CO_2$. For

399 immunofluorescence experiments, PC-12 cells were transfected with 3 μg plasmid and 9 μl

400 Lipofectamine 2000 in 300 μl Opti-MEM media for 6 hours. Cells were incubated at 37°C for 24

401 hours prior to testing for eGFP, Rab2a WT and Rab2a S20N expression. Cultured PC-12 cells were

16

402    treated with leupeptin (100 mM) or were mock treated for 24 h in growth medium before being

403    processed for CHGA immunostaining.

404    **Isolation and culture of mouse adrenal chromaffin cells**

405    Adrenal glands from 2-4 months old WT, *Lyz1$^{-/-}$, Nod1$^{-/-}$, Dbh-cre;Nod1$^{f/f}$* and *Nod1$^{f/f}$* mice were

406    used in each culture. Animals were anesthetized with $CO_2$, and the glands were isolated following

407    the procedures described by Aaron Kolski-Andreaco *et al.* (*Kolski-Andreaco, Cai, Currle, Chandy,*

408    *& Chow, 2007*). Glands were placed into a dish containing oxygenated Locke's buffer (NaCl 140

409    mM, KCl 5 mM, HEPES 10 mM, glucose 10 mM, $MgCl_2$ 1.2 mM, $CaCl_2$ 2.2 mM; pH7.35, osmolarity

410    between 295 and 300 mOsm.) on ice, and cortexes were removed. Adrenal medullas were digested

411    for 25 minutes twice in DMEM with papain (40 unit/ml), 1 mM $CaCl_2$ and 0.5 mM EDTA at 37°C.

412    Subsequently, the medullas were disrupted with a yellow tip in complete medium with DMEM, 5%

413    fetal calf serum,10% horse serum, and 5 µl/ml penicillin and streptomycin. Cells were pelleted for

414    8 minutes at 200 g. Pellets were resuspended in complete medium and plated on poly-L-lysine

415    pretreated coverslips or in imaging chambers. Primary adrenal chromaffin cells were then kept in

416    an incubator at 37°C with 5% $CO_2$.

417    **Amperometric recording and solutions**

418    Isolated chromaffin cells were obtained from the adrenal glands of adult (11-13 weeks old) WT,

419    *Lyz1$^{-/-}$* and *Nod1$^{-/-}$* male mice. Amperometric recordings were performed after 1-3 days in culture

420    at room temperature. The bath solution contained: 140 mM NaCl, 2.7 mM KCl, 5 mM $CaCl_2$, 1 mM

421    $MgCl_2$, 10 mM HEPES/NaOH, and 5-10 mM glucose. Osmolarity was around 300 mOsm, and the

422    pH was adjusted to 7.3 with NaOH. The working potential of the carbon fiber electrode (CFE) was

423    held at +700 mV with a patch-clamp amplifier (EPC10, HEKA, Germany). With a micromanipulator

424    (MPC200, Sutter Instruments, USA), the CFE was slowly advanced to the chromaffin cell of interest.

425    Data acquisition and analysis: The amperometric currents were recorded and analyzed using

426    the Quantal Analysis program in Igor Pro (Version 6.2, WaveMetrics, Lake Oswego, USA), written

17

427    by Drs. Mosharov and Sulzer (*Mosharov & Sulzer, 2005*). Data for off-line analysis were low-pass-

428    filtered at 1 kHz. A level of 5× the RMS of noise at baseline was set as the threshold for signal

429    detection.

430    ***Ex vivo* K$^+$-stimulated catecholamine secretion assay**

431    Cultured primary chromaffin cells were transfected following a published procedure (*Meunier et al.,*

432    *2013*). Briefly, primary chromaffin cells were plated into imaging chambers and allowed to adhere

433    for 3 hours. Complete medium was replaced with Opti-MEM medium, and the cells were transfected

434    with 1 µg GRAB$_{NE}$ using 2 µl Lipofectamine 2000. After 60 minutes, the mixture of Opti-MEM-

435    Lipofectamine-plasmid was replaced again by complete medium to end the transfection procedure.

436    The cells were used for secretion assay 48 hours later. In the experiment with chromaffin cells from

437    *Lyz1$^{-/-}$* mice, iE-DAP (1 µg/ml) was added into the complete medium 6 hours prior to the secretion

438    assay.

439    Cultured chromaffin cells from WT, *Lyz1$^{-/-}$, Nod1$^{-/-}$ Dbh-cre;Nod1$^{f/f}$* and *Nod1$^{f/f}$* mice

440    expressing the GRAB$_{NE}$ sensor were imaged using an inverted Ti-E A1 confocal microscope.

441    525/50 nm and 600/30 nm emission filters were used to collect the GFP and RFP signals.

442    Chromaffin cells expressing the GRAB$_{NE}$ sensor were first bathed in Tyrode's solution and imaged

443    during the course of the K$^+$ stimulation. The change in fluorescence intensity of the GRAB$_{NE}$ sensor

444    was calculated by recording the changes in the green and red fluorescence. For the recording, the

445    exposure time was set at 50 ms per frame and the acquisition frequency was imaging every 5

446    seconds to reduce light bleaching. The solution used for perfusion was the physiological solution

447    Tyrode's solution (adjusted to pH=7.3-7.4), and KCl was added to reach a concentration of 90 mM.

448    The average fluorescence intensity at the five time points before K$^+$ stimulation was defined as F0.

449    The instantaneous ΔF/F0 was calculated as (Ft - F0)/F0.

**Measurement of epinephrine in mouse plasma and tissue**

450

451    Whole adrenal glands from WT, *Lyz1⁻/⁻, Nod1⁻/⁻, Dbh-cre;Nod1^{f/f}, Nod1^{f/f}* and ABX mice (ABX mice

452    were prepared according to the published procedure (*Hill et al., 2010*)) were dissected on an ice

453    bath. Subsequently, the isolated adrenal glands were weighed and homogenized with acetonitrile

454    (30 µl for every 1 mg of tissue). Ascorbic acid (final concentration at 3 mg/ml) was added as

455    antioxidant into the acetonitrile. After thorough homogenization, samples were subjected to

456    sonication for 60 seconds to fully extract catecholamines. The adrenal gland homogenates were

457    centrifuged at 12,000 rpm for 10 minutes at 4°C. Supernatants were collected and stored at -80°C

458    before quantification.

459        Mice were subjected to restraint stress in a piping bag for 25 minutes or 1 hour at 8 am. A hole

460    was made in the tip of the piping bag to enable air flow. Animals could move their heads but were

461    unable to move their arms and legs. For the control group, the mice were placed in the home cage

462    at the same time without food and water. Rectal temperature and blood glucose readings were

463    taken before and after the restraint. Blood samples were collected into tubes containing 5 mM

464    EDTA through orbital sinus bleeding. Subsequently, the samples were centrifuged and the plasma

465    samples were stored at -80°C before analysis.

466        The concentration of epinephrine in tissue or plasma samples was measured using an

467    Adrenaline Research Elisa kit (BA E-5100) from Labor Diagnostika Nord.

**Immunofluorescence staining of PC-12 cells or primary chromaffin cells**

468

469    Cells grown on coverslips were washed with cold PBS and fixed in 4% PFA for 15 minutes at 4°C.

470    Cells were then washed three times with PBS and blocked with antibody dilution buffer (PBS

471    supplemented with 5% goat serum and 0.1% saponin) for 30 minutes. Cells were incubated with

472    primary antibodies at 4°C overnight followed by fluorophore-conjugated secondary antibodies at

473    RT for 2 hours. Samples were washed in PBS containing 0.1% Tween-20 three times for each step.

474    Antibody dilution buffer was used throughout for antibody incubation steps. Coverslips were then

19

475    counterstained and mounted onto slides in Fluoromount-G. Confocal images were obtained with a

476    Zeiss LSM 710 imaging system under a 63x oil objective.

**Immunofluorescence (IF) staining of tissue sections**

478    Murine tissues were fixed in 4% PFA/PBS overnight, dehydrated and embedded in paraffin. Tissue

479    slices (6 μm in thickness) were mounted on positively charged glass and dewaxed. Antigen retrieval

480    was performed by incubation in 0.01 M sodium citrate buffer (pH6.0) for 25 minutes in a boiling

481    steamer. For immunofluorescence staining, slides were then blocked with normal goat serum

482    blocking reagent for 30 minutes, followed by sequential incubation with primary antibodies at 4°C

483    overnight and fluorophore-conjugated secondary antibodies at RT for 2 h. Slides were then

484    counterstained with DAPI and mounted in Fluor mount-G. Confocal images were obtained with

485    Zeiss LSM 710 or Nikon Ti NE imaging systems.

486    For immunohistochemistry staining, slides were then treated with an UltraSensitive TM S-P Kit

487    instead. After sequential incubation with hydrogen peroxide (~ 15 minutes), blocking serum (~ 20

488    minutes), primary antibodies (overnight at 4°C), biotinylated secondary antibody (~ 20 minutes) and

489    streptavidin-peroxidase (~ 20 minutes), immunoreactivity was visualized using diaminobenzidine

490    (DAB). The slides were counterstained with hematoxylin, mounted, and observed with a light

491    microscope (Nikon Eclipse 90i).

**Gene expression analysis using quantitative reverse-transcription PCR**

493    RNA was extracted from dissected adrenal medulla and stored in Trizol at -80°C. RNA was then

494    quantified and purified with a PrimerScript RT reagent kit. q-PCR reactions were performed with

495    SYRB Premix Taq on a Rotor Gene 6000 thermal cycler in triplicate. The following thermal cycling

496    conditions were used: 95°C for 30 seconds, followed by 40 cycles of 95°C for 5 seconds and 60°C

497    for 34 seconds. The specificity of q-PCR was verified with melting curves for each PCR reaction.

498    The level of target mRNA was determined by Delta-Delta Ct values between the target and loading

499    control. Primers for q-PCR are listed in the Supplementary Information.

**Western blotting**

The dissected adrenal medullas were homogenized in RIPA buffer (150 mM NaCl, 1% NP-40, 0.5% sodium deoxycholate, 0.1% SDS, 50 mM Tris pH8.0, 5.0 mM EDTA pH8.0, 0.5 mM dithiothreitol) supplemented with a protease inhibitor cocktail and 10 mM PMSF. The lysates were placed on ice for 30 minutes, then centrifuged at 12,000 rpm (10 minutes) to remove cell debris. Equal amounts of protein were separated on SDS-PAGE gels and blotted onto immobilon-p PVDF membranes. After blocking in 5% skim milk in PBS-T (0.5% Tween-20) for 1 hour at room temperature, membranes were incubated with primary antibody at 4°C overnight and secondary HRP-conjugated antibodies and visualized by using ECL detection reagent. Protein band intensity was quantified using ImageJ software.

**Electron microscopic analyses of DCGs in adrenal chromaffin cells**

Isolated adrenal glands from euthanized mice were washed with cold PBS and cut into halves. Tissues were then fixed in 0.1 M sodium phosphate buffer (pH7.2) containing 2.5% glutaraldehyde and 2% paraformaldehyde at 4°C overnight. Dehydration was performed with an ethanol gradient followed by infiltration and embedding with a SPI-Pon 812 Epoxy Embedding Kit. Sections were cut on a Leica Ultracut Ultramicrotome (Leica EM UC6) and stained with uranyl acetate and lead citrate. The digital images were obtained under a transmission electron microscope (Hitichi H-7650) at 80 kV.

For morphometric analysis, the diameters and densities of typical and atypical dense core granules were measured using ImageJ software.

**Statistical analysis**

Statistical analysis was performed using GraphPad Prism 8.1. Statistical tests were performed by GraphPad Prism. Student's *t*-test was used for comparisons between two groups. One-way ANOVA was used for comparisons between more than two groups. The respective statistical test

21

524    used for each figure is noted in the corresponding figure legends and significant statistical

525    differences are noted as ns *(p>0.05), *p≤0.05, **p≤0.01, ***p≤0.001, ****p≤0.0001.*

536

537    **Competing interests**

538    No competing interests declared.

539    **References**

540    Ailion, M., Hannemann, M., Dalton, S., Pappas, A., Watanabe, S., Hegermann, J., . . . Jorgensen,
541        E. M. (2014). Two Rab2 interactors regulate dense-core vesicle maturation. *Neuron, 82*(1), 167-
542        180. doi:10.1016/j.neuron.2014.02.017
543    Arentsen, T., Qian, Y., Gkotzis, S., Femenia, T., Wang, T., Udekwu, K., . . . Diaz Heijtz, R. (2017).
544        The bacterial peptidoglycan-sensing molecule Pglyrp2 modulates brain development and
545        behavior. *Mol Psychiatry, 22*(2), 257-266. doi:10.1038/mp.2016.182
546    Axelrod, J., & Weinshilboum, R. (1972). Catecholamines. *287*(5), 237-242.
547        doi:10.1056/nejm197208032870508
548    Berends, A. M. A., Eisenhofer, G., Fishbein, L., Horst-Schrivers, A., Kema, I. P., Links, T. P., . . .
549        Kerstens, M. N. (2019). Intricacies of the Molecular Machinery of Catecholamine Biosynthesis
550        and Secretion by Chromaffin Cells of the Normal Adrenal Medulla and in Pheochromocytoma
551        and Paraganglioma. *Cancers (Basel), 11*(8). doi:10.3390/cancers11081121
552    Bird, L. (2010). A NOD to neutrophils. *Nature Reviews Immunology, 10*(3), 157-157.
553        doi:10.1038/nri2739
554    Blander, J. M., Longman, R. S., Iliev, I. D., Sonnenberg, G. F., & Artis, D. (2017). Regulation of
555        inflammation by microbiota interactions with the host. *Nat Immunol, 18*(8), 851-860.
556        doi:10.1038/ni.3780
557    Bonham, K. S., & Kagan, J. C. (2014). Endosomes as Platforms for NOD-like Receptor Signaling.
558        *Cell Host & Microbe, 15*(5), 523-525. doi:10.1016/j.chom.2014.05.001

559  Bornstein, S. R., Zacharowski, P., Schumann, R. R., Barthel, A., Tran, N., Papewalis, C., . . .
560      Zacharowski, K. (2004). Impaired adrenal stress response in Toll-like receptor 2-deficient mice.
561      *Proc Natl Acad Sci U S A, 101*(47), 16695-16700. doi:10.1073/pnas.0407550101
562  Brinkman, D. J., Ten Hove, A. S., Vervoordeldonk, M. J., Luyer, M. D., & de Jonge, W. J. (2019).
563      Neuroimmune Interactions in the Gut and Their Significance for Intestinal Immunity. *Cells, 8*(7).
564      doi:10.3390/cells8070670
565  Buffa, L., Fuchs, E., Pietropaolo, M., Barr, F., & Solimena, M. (2008). ICA69 is a novel Rab2 effector
566      regulating ER-Golgi trafficking in insulinoma cells. *Eur J Cell Biol, 87*(4), 197-209.
567      doi:10.1016/j.ejcb.2007.11.003
568  Buira, I., Poch, E., Sanchez, O., Fernandez-Varo, G., Grau, M., Tebar, F., . . . Soley, M. (2004).
569      Sialoadenectomy alters liver cell turn-over and function in mice. *Journal of Cellular Physiology,*
570      *198*(1), 12-21. doi:10.1002/jcp.10402
571  Cadwell, K. (2016). Crosstalk between autophagy and inflammatory signalling pathways: balancing
572      defence     and     homeostasis.     *Nature     Reviews     Immunology,     16*(11),     661-675.
573      doi:10.1038/nri.2016.100
574  Cannon, W. B. (1914). The emergency function of the adrenal medulla in pain and the major
575      emotions. *American Journal of Physiology-Legacy Content, 33*(2), 356-372.
576  Chamaillard, M., Hashimoto, M., Horie, Y., Masumoto, J., Qiu, S., Saab, L., . . . Inohara, N. (2003).
577      An essential role for NOD1 in host recognition of bacterial peptidoglycan containing
578      diaminopimelic acid. *Nat Immunol, 4*(7), 702-707. doi:10.1038/ni945
579  Chu, H., Khosravi, A., Kusumawardhani, I. P., Kwon, A. H., Vasconcelos, A. C., Cunha, L. D., . . .
580      Mazmanian, S. K. (2016). Gene-microbiota interactions contribute to the pathogenesis of
581      inflammatory bowel disease. *Science, 352*(6289), 1116-1120. doi:10.1126/science.aad9948
582  Clarke, T. B., Davis, K. M., Lysenko, E. S., Zhou, A. Y., Yu, Y., & Weiser, J. N. (2010). Recognition
583      of peptidoglycan from the microbiota by Nod1 enhances systemic innate immunity. *Nature*
584      *Medicine, 16*(2), 228-231. doi:10.1038/nm.2087
585  Crumeyrolle-Arias, M., Jaglin, M., Bruneau, A., Vancassel, S., Cardona, A., Dauge, V., . . . Rabot,
586      S. (2014). Absence of the gut microbiota enhances anxiety-like behavior and neuroendocrine
587      response    to    acute    stress    in    rats.    *Psychoneuroendocrinology,    42*,    207-217.
588      doi:10.1016/j.psyneuen.2014.01.014
589  Díaz-Vera, J., Camacho, M., Machado, J. D., Domínguez, N., Montesinos, M. S., Hernández-
590      Fernaud, J. R., . . . Borges, R. (2012). Chromogranins A and B are key proteins in amine
591      accumulation, but the catecholamine secretory pathway is conserved without them. *The FASEB*
592      *Journal, 26*(1), 430-438. doi:10.1096/fj.11-181941
593  Diaz Heijtz, R., Wang, S., Anuar, F., Qian, Y., Bjorkholm, B., Samuelsson, A., . . . Pettersson, S.
594      (2011). Normal gut microbiota modulates brain development and behavior. *Proc Natl Acad Sci U*
595      *S A, 108*(7), 3047-3052. doi:10.1073/pnas.1010529108
596  Dunevall, J., Fathali, H., Najafinobar, N., Lovric, J., Wigstrom, J., Cans, A. S., & Ewing, A. G. (2015).
597      Characterizing the catecholamine content of single mammalian vesicles by collision-adsorption
598      events at an electrode. *J Am Chem Soc, 137*(13), 4344-4346. doi:10.1021/ja512972f
599  Edwards, S. L., Charlie, N. K., Richmond, J. E., Hegermann, J., Eimer, S., & Miller, K. G. (2009).
600      Impaired dense core vesicle maturation inCaenorhabditis elegansmutants lacking Rab2. *The*
601      *Journal of Cell Biology, 186*(6), 881-895. doi:10.1083/jcb.200902095
602  Eisenhofer, G., Kopin, I. J., & Goldstein, D. S. (2004). Catecholamine metabolism: a contemporary
603      view    with    implications    for    physiology    and    medicine.    *Pharmacol Rev, 56*(3),    331-349.
604      doi:10.1124/pr.56.3.1
605  El-Salhy, M., Solomon, T., Hausken, T., Gilja, O. H., & Hatlebakk, J. G. (2017). Gastrointestinal
606      neuroendocrine peptides/amines in inflammatory bowel disease. *World J Gastroenterol, 23*(28),
607      5068-5085. doi:10.3748/wjg.v23.i28.5068
608  Farzi, A., Frohlich, E. E., & Holzer, P. (2018). Gut Microbiota and the Neuroendocrine System.
609      *Neurotherapeutics, 15*(1), 5-22. doi:10.1007/s13311-017-0600-5
610  Farzi, A., Reichmann, F., Meinitzer, A., Mayerhofer, R., Jain, P., Hassan, A. M., . . . Holzer, P. (2015).
611      Synergistic effects of NOD1 or NOD2 and TLR4 activation on mouse sickness behavior in relation
612      to    immune    and    brain    activity    markers.    *Brain    Behav    Immun,    44*,    106-120.

613      doi:10.1016/j.bbi.2014.08.011

614 Feng, J., Zhang, C., Lischinsky, J. E., Jing, M., Zhou, J., Wang, H., . . . Li, Y. (2019). A Genetically
615      Encoded Fluorescent Sensor for Rapid and Specific In Vivo Detection of Norepinephrine. *Neuron,*
616      *102*(4), 745-761.e748. doi:10.1016/j.neuron.2019.02.037

617 Fernandez, G., Mena, M. P., Arnau, A., Sanchez, O., Soley, M., & Ramirez, I. (2000). Immobilization
618      stress induces c-Fos accumulation in liver. *Cell Stress Chaperones, 5*(4), 306-312.
619      doi:10.1379/1466-1268(2000)005<0306:isicfa>2.0.co;2

620 Foster, J. A., & McVey Neufeld, K. A. (2013). Gut-brain axis: how the microbiome influences anxiety
621      and depression. *Trends Neurosci, 36*(5), 305-312. doi:10.1016/j.tins.2013.01.005

622 Fung, T. C., Olson, C. A., & Hsiao, E. Y. (2017). Interactions between the microbiota, immune and
623      nervous systems in health and disease. *Nat Neurosci, 20*(2), 145-155. doi:10.1038/nn.4476

624 Garcia, A. G., Garcia-De-Diego, A. M., Gandia, L., Borges, R., & Garcia-Sancho, J. (2006). Calcium
625      signaling and exocytosis in adrenal chromaffin cells. *Physiol Rev, 86*(4), 1093-1131.
626      doi:10.1152/physrev.00039.2005

627 Gerfen, C. R., Paletzki, R., & Heintz, N. (2013). GENSAT BAC cre-recombinase driver lines to study
628      the functional organization of cerebral cortical and basal ganglia circuits. *Neuron, 80*(6), 1368-
629      1383. doi:10.1016/j.neuron.2013.10.016

630 Giri, P., Hu, F., La Gamma, E. F., & Nankova, B. B. (2019). Absence of gut microbial colonization
631      attenuates the sympathoadrenal response to hypoglycemic stress in mice: implications for
632      human neonates. *Pediatr Res, 85*(4), 574-581. doi:10.1038/s41390-018-0270-y

633 Greene, L. A., & Tischler, A. S. (1976). Establishment of a Noradrenergic Clonal Line of Rat Adrenal
634      Pheochromocytoma Cells Which Respond to Nerve Growth-Factor. *Proceedings of the National*
635      *Academy of Sciences of the United States of America, 73*(7), 2424-2428. doi:DOI
636      10.1073/pnas.73.7.2424

637 Hergott, C. B., Roche, A. M., Tamashiro, E., Clarke, T. B., Bailey, A. G., Laughlin, A., . . . Weiser, J.
638      N. (2016). Peptidoglycan from the gut microbiota governs the lifespan of circulating phagocytes
639      at homeostasis. *Blood, 127*(20), 2460-2471. doi:10.1182/blood-2015-10-675173

640 Hill, D. A., Hoffmann, C., Abt, M. C., Du, Y., Kobuley, D., Kirn, T. J., . . . Artis, D. (2010). Metagenomic
641      analyses reveal antibiotic-induced temporal and spatial changes in intestinal microbiota with
642      associated alterations in immune cell homeostasis. *Mucosal Immunol, 3*(2), 148-158.
643      doi:10.1038/mi.2009.132

644 Huo, R., Zeng, B., Zeng, L., Cheng, K., Li, B., Luo, Y., . . . Xie, P. (2017). Microbiota Modulate
645      Anxiety-Like Behavior and Endocrine Abnormalities in Hypothalamic-Pituitary-Adrenal Axis.
646      *Front Cell Infect Microbiol, 7*, 489. doi:10.3389/fcimb.2017.00489

647 Inohara, N., Koseki, T., del Peso, L., Hu, Y., Yee, C., Chen, S., . . . Nunez, G. (1999). Nod1, an
648      Apaf-1-like activator of caspase-9 and nuclear factor-kappaB. *Journal of Biological Chemistry,*
649      *274*(21), 14560-14567. doi:10.1074/jbc.274.21.14560

650 Inohara, N., & Nunez, G. (2003). NODs: intracellular proteins involved in inflammation and
651      apoptosis. *Nat Rev Immunol, 3*(5), 371-382. doi:10.1038/nri1086

652 Jirout, M. L., Friese, R. S., Mahapatra, N. R., Mahata, M., Taupenot, L., Mahata, S. K., . . . O'Connor,
653      D. T. (2010). Genetic regulation of catecholamine synthesis, storage and secretion in the
654      spontaneously hypertensive rat. *Hum Mol Genet, 19*(13), 2567-2580. doi:10.1093/hmg/ddq135

655 Kang, Y. J., Sim, Y. B., Park, S. H., Sharma, N., & Suh, H. W. (2015). Involvement of alpha(2)-
656      adrenergic receptor in the regulation of the blood glucose level induced by immobilization stress.
657      *Arch Pharm Res, 38*(5), 921-929. doi:10.1007/s12272-014-0430-5

658 Khani, S., & Tayek, J. A. (2001). Cortisol increases gluconeogenesis in humans: its role in the
659      metabolic syndrome. *Clin Sci (Lond), 101*(6), 739-747. doi:10.1042/cs1010739

660 Kim, T., Tao-Cheng, J. H., Eiden, L. E., & Loh, Y. P. (2001). Chromogranin A, an "on/off" switch
661      controlling dense-core secretory granule biogenesis. *Cell, 106*(4), 499-509. doi:10.1016/s0092-
662      8674(01)00459-7

663 Kim, T., Zhang, C. F., Sun, Z., Wu, H., & Loh, Y. P. (2005). Chromogranin A deficiency in transgenic
664      mice leads to aberrant chromaffin granule biogenesis. *J Neurosci, 25*(30), 6958-6961.
665      doi:10.1523/JNEUROSCI.1058-05.2005

666 Kolski-Andreaco, A., Cai, H., Currle, D. S., Chandy, K. G., & Chow, R. H. (2007). Mouse Adrenal

667        Chromaffin Cell Isolation. *Journal of Visualized Experiments*(2). doi:10.3791/129

668 Liu, J., Buisman-Pijlman, F., & Hutchinson, M. R. (2014). Toll-like receptor 4: innate immune
669        regulator of neuroimmune and neuroendocrine interactions in stress and major depressive
670        disorder. *Front Neurosci, 8*, 309. doi:10.3389/fnins.2014.00309

671 Lu, Y., Zheng, Y. P., Coyaud, E., Zhang, C., Selvabaskaran, A., Yu, Y. Y., . . . Neculai, D. (2019).
672        Palmitoylation of NOD1 and NOD2 is required for bacterial sensing. *Science, 366*(6464), 460-+.
673        doi:10.1126/science.aau6391

674 Luo, Y., Zeng, B., Zeng, L., Du, X., Li, B., Huo, R., . . . Xie, P. (2018). Gut microbiota regulates
675        mouse behaviors through glucocorticoid receptor pathway genes in the hippocampus. *Transl*
676        *Psychiatry, 8*(1), 187. doi:10.1038/s41398-018-0240-5

677 Mahapatra, N. R., Mahata, M., Hazra, P. P., McDonough, P. M., O'Connor, D. T., & Mahata, S. K.
678        (2004). A dynamic pool of calcium in catecholamine storage vesicles. Exploration in living cells
679        by a novel vesicle-targeted chromogranin A-aequorin chimeric photoprotein. *Journal of Biological*
680        *Chemistry, 279*(49), 51107-51121. doi:10.1074/jbc.M408742200

681 Meunier, F. A., Álvarez, Y. D., Belingheri, A. V., Perez Bay, A. E., Javis, S. E., Tedford, H. W., . . .
682        Marengo, F. D. (2013). The Immediately Releasable Pool of Mouse Chromaffin Cell Vesicles Is
683        Coupled to P/Q-Type Calcium Channels via the Synaptic Protein Interaction Site. *PLoS One,*
684        *8*(1). doi:10.1371/journal.pone.0054846

685 Mogensen, T. H. (2009). Pathogen recognition and inflammatory signaling in innate immune
686        defenses. *Clin Microbiol Rev, 22*(2), 240-273, Table of Contents. doi:10.1128/CMR.00046-08

687 Mosharov, E. V., & Sulzer, D. (2005). Analysis of exocytotic events recorded by amperometry. *Nat*
688        *Methods, 2*(9), 651-658. doi:10.1038/nmeth782

689 Muller, A., Joseph, V., Slesinger, P. A., & Kleinfeld, D. (2014). Cell-based reporters reveal in vivo
690        dynamics of dopamine and norepinephrine release in murine cortex. *Nat Methods, 11*(12), 1245-
691        1252. doi:10.1038/nmeth.3151

692 Nakamura, N., Lill, J. R., Phung, Q., Jiang, Z. S., Bakalarski, C., de Maziere, A., . . . Mellman, I.
693        (2014). Endosomes are specialized platforms for bacterial sensing and NOD2 signalling. *Nature,*
694        *509*(7499), 240-+. doi:10.1038/nature13133

695 Nicholson, J. K., Holmes, E., Kinross, J., Burcelin, R., Gibson, G., Jia, W., & Pettersson, S. (2012).
696        Host-gut microbiota metabolic interactions. *Science, 336*(6086), 1262-1267.
697        doi:10.1126/science.1223813

698 Padgett, D. A., & Glaser, R. (2003). How stress influences the immune response. *Trends in*
699        *Immunology, 24*(8), 444-448. doi:10.1016/s1471-4906(03)00173-x

700 Park, S.-H., Sim, Y.-B., Kim, S.-S., Lee, J.-R., Sharma, N., & Suh, H.-W. (2016). Effects of 5,7-
701        dihydroxytryptamine administered supraspinally or spinally on the blood glucose level in D-glucose-
702        fed and immobilization stress models. *Animal Cells and Systems, 20*(5), 289-295.
703        doi:10.1080/19768354.2016.1221854

704 Pasqua, T., Mahata, S., Bandyopadhyay, G. K., Biswas, A., Perkins, G. A., Sinha-Hikim, A. P., . . .
705        Mahata, S. K. (2016). Impact of Chromogranin A deficiency on catecholamine storage,
706        catecholamine granule morphology and chromaffin cell energy metabolism in vivo. *Cell Tissue*
707        *Res, 363*(3), 693-712. doi:10.1007/s00441-015-2316-3

708 Pusceddu, M. M., Barboza, M., Keogh, C. E., Schneider, M., Stokes, P., Sladek, J. A., . . . Gareau,
709        M. G. (2019). Nod-like receptors are critical for gut-brain axis signalling in mice. *J Physiol,*
710        *597*(24), 5777-5797. doi:10.1113/JP278640

711 Robinson, D. L., Venton, B. J., Heien, M. L. A. V., & Wightman, R. M. (2003). Detecting Subsecond
712        Dopamine Release with Fast-Scan Cyclic Voltammetry in Vivo. *49*(10), 1763-1773.
713        doi:10.1373/49.10.1763 %J Clinical Chemistry

714 Rogers, G. B., Keating, D. J., Young, R. L., Wong, M. L., Licinio, J., & Wesselingh, S. (2016). From
715        gut dysbiosis to altered brain function and mental illness: mechanisms and pathways. *Mol*
716        *Psychiatry, 21*(6), 738-748. doi:10.1038/mp.2016.50

717 Rooks, M. G., & Garrett, W. S. (2016). Gut microbiota, metabolites and host immunity. *Nat Rev*
718        *Immunol, 16*(6), 341-352. doi:10.1038/nri.2016.42

719 Schneider, M., Zhang, N., Barrett, K., & Gareau, M. (2016). Nod Receptors Modulate the
720        Microbiota-Gut-Brain Axis. *Inflammatory Bowel Diseases, 22*, S66-S66. doi:Doi

721      10.1097/01.Mib.0000480290.04728.59

722 Shanks, N., Larocque, S., & Meaney, M. J. (1995). Neonatal Endotoxin Exposure Alters the
723      Development of the Hypothalamic-Pituitary-Adrenal Axis - Early Illness and Later Responsivity
724      to Stress. *Journal of Neuroscience, 15*(1), 376-384. doi:DOI 10.1523/jneurosci.15-01-
725      00376.1995

726 Ste Marie, L., & Palmiter, R. D. (2003). Norepinephrine and epinephrine-deficient mice are
727      hyperinsulinemic and have lower blood glucose. *Endocrinology, 144*(10), 4427-4432.
728      doi:10.1210/en.2003-0561

729 Sudo, N., Chida, Y., Aiba, Y., Sonoda, J., Oyama, N., Yu, X. N., . . . Koga, Y. (2004). Postnatal
730      microbial colonization programs the hypothalamic-pituitary-adrenal system for stress response
731      in mice. *J Physiol, 558*(Pt 1), 263-275. doi:10.1113/jphysiol.2004.063388

732 Sugawara, T., Kano, F., & Murata, M. (2014). Rab2A is a pivotal switch protein that promotes either
733      secretion or ER-associated degradation of (pro)insulin in insulin-secreting cells. *Sci Rep, 4*, 6952.
734      doi:10.1038/srep06952

735 Sumakovic, M., Hegermann, J., Luo, L., Husson, S. J., Schwarze, K., Olendrowitz, C., . . . Eimer,
736      S. (2009). UNC-108/RAB-2 and its effector RIC-19 are involved in dense core vesicle maturation
737      in Caenorhabditis elegans. *J Cell Biol, 186*(6), 897-914. doi:10.1083/jcb.200902096

738 Tank, A. W., & Lee Wong, D. (2015). Peripheral and central effects of circulating catecholamines.
739      *Compr Physiol, 5*(1), 1-15. doi:10.1002/cphy.c140007

740 Tisdale, E. J., Bourne, J. R., Khosravi-Far, R., Der, C. J., & Balch, W. E. (1992). GTP-binding
741      mutants of rab1 and rab2 are potent inhibitors of vesicular transport from the endoplasmic
742      reticulum to the Golgi complex. *The Journal of Cell Biology, 119*(4), 749-761.
743      doi:10.1083/jcb.119.4.749

744 Travassos, L. H., Carneiro, L. A., Ramjeet, M., Hussey, S., Kim, Y. G., Magalhaes, J. G., . . . Philpott,
745      D. J. (2010). Nod1 and Nod2 direct autophagy by recruiting ATG16L1 to the plasma membrane
746      at the site of bacterial entry. *Nat Immunol, 11*(1), 55-62. doi:10.1038/ni.1823

747 Tsigos, C., & Chrousos, G. P. (2002). Hypothalamic-pituitary-adrenal axis, neuroendocrine factors
748      and stress. *J Psychosom Res, 53*(4), 865-871. doi:10.1016/s0022-3999(02)00429-4

749 Videen, J. S., Mezger, M. S., Chang, Y. M., & O'Connor, D. T. (1992). Calcium and catecholamine
750      interactions with adrenal chromogranins. Comparison of driving forces in binding and
751      aggregation. *Journal of Biological Chemistry, 267*(5), 3066-3073. Retrieved from
752      https://www.ncbi.nlm.nih.gov/pubmed/1737762

753 Wang, H., Jing, M., & Li, Y. (2018). Lighting up the brain: genetically encoded fluorescent sensors
754      for imaging neurotransmitters and neuromodulators. *Current Opinion in Neurobiology, 50*, 171-
755      178. doi:10.1016/j.conb.2018.03.010

756 Wightman, R. M., Jankowski, J. A., Kennedy, R. T., Kawagoe, K. T., Schroeder, T. J., Leszczyszyn,
757      D. J., . . . Viveros, O. H. (1991). Temporally resolved catecholamine spikes correspond to single
758      vesicle release from individual chromaffin cells. *Proc Natl Acad Sci U S A, 88*(23), 10754-10758.
759      doi:10.1073/pnas.88.23.10754

760 Zacharowski, K., Zacharowski, P. A., Koch, A., Baban, A., Tran, N., Berkels, R., . . . Bornstein, S.
761      R. (2006). Toll-like receptor 4 plays a crucial role in the immune-adrenal response to systemic
762      inflammatory response syndrome. *Proc Natl Acad Sci U S A, 103*(16), 6392-6397.
763      doi:10.1073/pnas.0601527103

764 Zhang, Q., Pan, Y., Yan, R., Zeng, B., Wang, H., Zhang, X., . . . Liu, Z. (2015). Commensal bacteria
765      direct selective cargo sorting to promote symbiosis. *Nat Immunol, 16*(9), 918-926.
766      doi:10.1038/ni.3233

767 Zhang, Q., Pan, Y., Zeng, B., Zheng, X., Wang, H., Shen, X., . . . Liu, Z. (2019). Intestinal lysozyme
768      liberates Nod1 ligands from microbes to direct insulin trafficking in pancreatic beta cells. *Cell Res,*
769      *29*(7), 516-532. doi:10.1038/s41422-019-0190-3

770 Zheng, P., Zeng, B., Zhou, C., Liu, M., Fang, Z., Xu, X., . . . Xie, P. (2016). Gut microbiome
771      remodeling induces depressive-like behaviors through a pathway mediated by the host's
772      metabolism. *Mol Psychiatry, 21*(6), 786-796. doi:10.1038/mp.2016.44
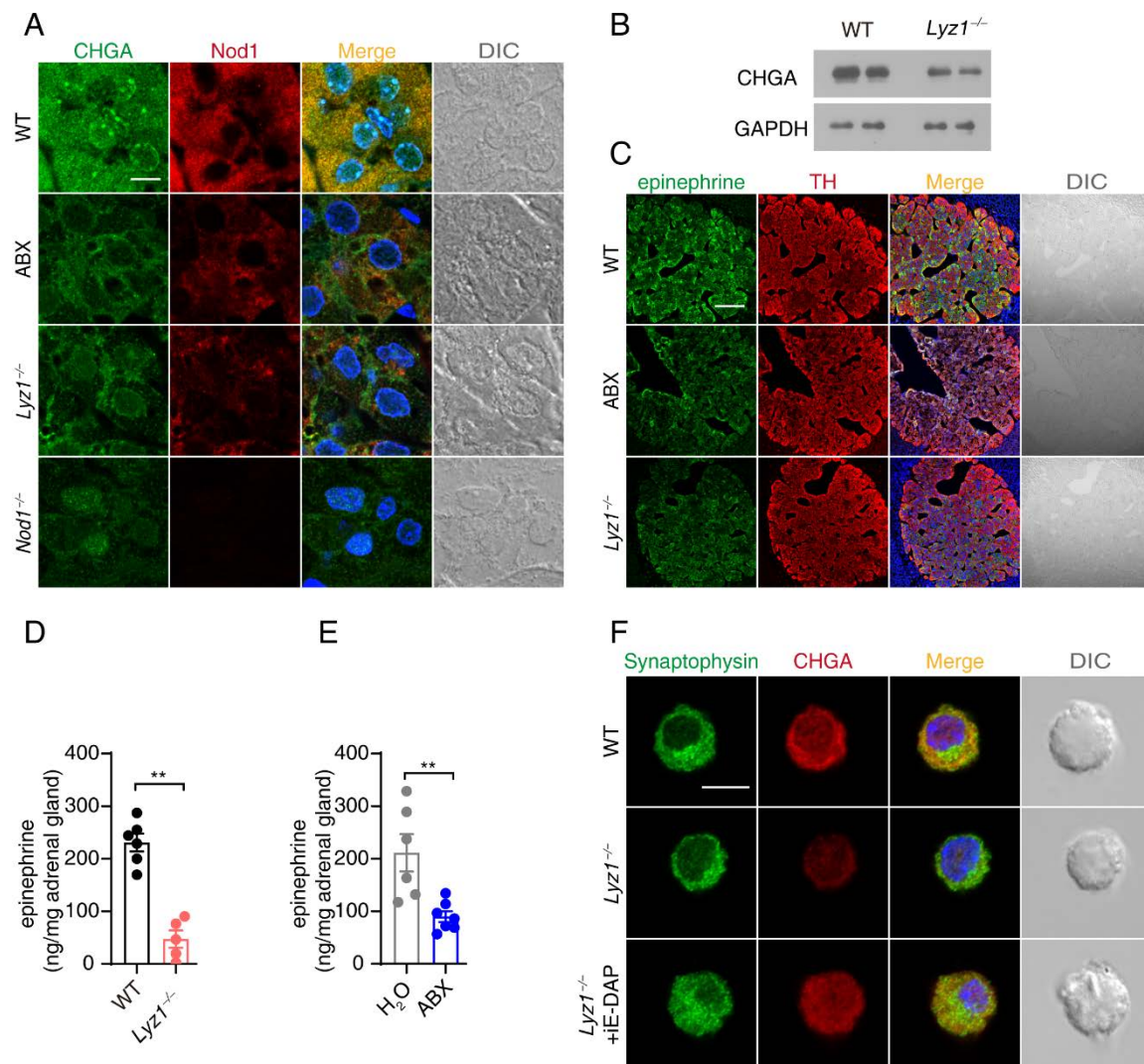
**Figure 1**
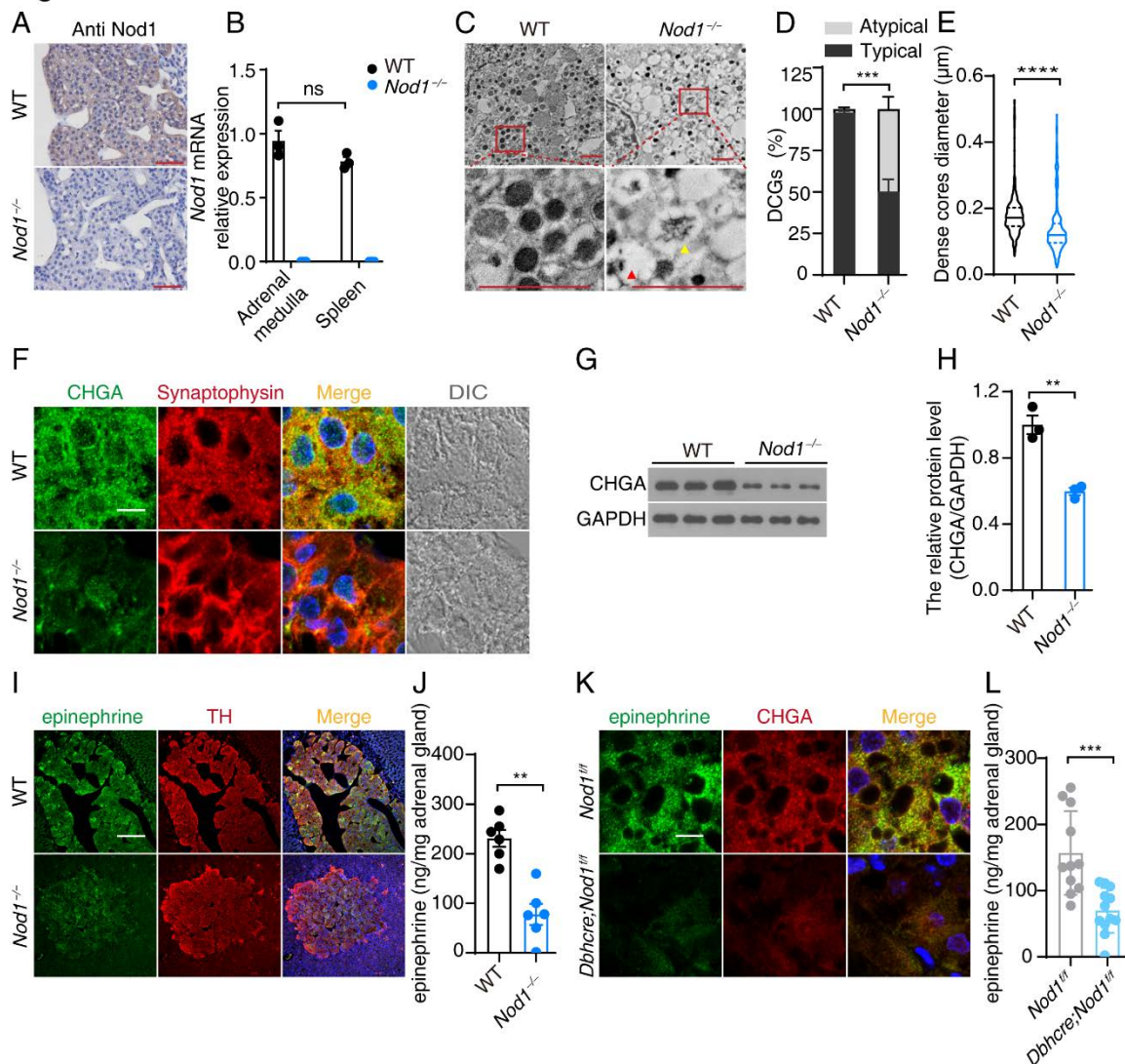


**Figure 1.** Adrenal chromaffin cells sense microbial signals in a Nod1-dependent manner. (**A**) Immunohistochemical staining (IHC) of Nod1 in paraffin sections of adrenal glands from wild-type (WT) and *Nod1*$^{-/-}$ mice. (**B**) Relative *Nod1* mRNA levels in adrenal medulla and spleen determined by qPCR. The *GAPDH* mRNA level was used for normalization. (**C**) Electron microscopy images of adrenal chromaffin cells from WT and *Nod1*$^{-/-}$ mice. Boxed areas are shown at higher magnification in the panels immediately below to indicate the atypical dense core granules (DCGs) in *Nod1*$^{-/-}$ mice. (**D**) Quantification of DCGs in WT and *Nod1*$^{-/-}$ mice from EM images as shown in (**C**). Atypical dense core granules were defined as those with a decreased dense core, as indicated by the yellow triangle in (**C**), or with no noticeable dense core, as indicated by the red triangle in (**C**). A total of approximately 300 DCGs from 2 adrenal gland of each genotype were used for quantification. (**E**) The diameters of DCGs in WT and *Nod1*$^{-/-}$ mice. (**F**) Immunostaining and confocal imaging of CHGA (green) and synaptophysin (red) in paraffin sections of adrenal gland

27

785   from WT and *Nod1*$^{-/-}$ mice. (**G**, **H**) Representative immunoblots (**G**) and quantification (**H**) of CHGA

786   in dissected adrenal medullas from WT and *Nod1*$^{-/-}$ mice (n=3). GAPDH was used as loading

787   control. (**I**) Immunostaining and confocal imaging of epinephrine (green) and tyrosine hydroxylase

788   (TH, red) in paraffin sections of adrenal gland from WT and *Nod1*$^{-/-}$ mice. (**J**) Adrenal gland

789   epinephrine content in WT and *Nod1*$^{-/-}$ mice. (**K**) Immunostaining and confocal imaging of

790   epinephrine (green) and CHGA (red) in paraffin sections of adrenal gland from *Nod1*$^{f/f}$ and *Dbh-*

791   *cre;Nod1*$^{f/f}$ mice. (**L**) Adrenal gland epinephrine content in *Nod1*$^{f/f}$ and *Dbh-cre;Nod1*$^{f/f}$ mice. Scale

792   bars, 10 µm (**F**, **K**); 1 µm (**C**); 50 µm (**A**, **I**). Violin plots show median and quartile (**E**). Summary

793   plots show all data points with mean and s.e.m.; each symbol represents an individual mouse (**B**,

794   **H**, **J**, **L**). Statistically significant differences were determined using the Mann-Whitney test (**B**, **D**, **J**,

795   **L**), unpaired student *t test* (**H**) or Kolmogorov-Smirnov test for cumulative distribution (**E**). *\*\*p*<0.01,

796   *\*\*\*p*<0.001 and *\*\*\*\*p*<0.0001*.* Data (**A**-**L**) are representative of three independent experiments.

**Figure 2.** Microbial Nod1 ligand regulates the amount of CHGA and epinephrine in DCGs. (**A**) Immunostaining and confocal imaging of CHGA (green) and Nod1 (red) in paraffin sections of adrenal gland from WT, ABX, *Lyz1*$^{-/-}$ and *Nod1*$^{-/-}$ mice. (**B**) Representative immunoblots of CHGA in the dissected adrenal medullas from WT and *Lyz1*$^{-/-}$ mice. GAPDH was used as loading control. (**C**) Immunostaining and confocal imaging of epinephrine (green) and TH (red) in paraffin sections of adrenal gland from WT, ABX and *Lyz1*$^{-/-}$ mice. (**D**) The epinephrine content in adrenal glands from WT (n=6) and *Lyz1*$^{-/-}$ (n=5) mice. (**E**) The epinephrine content in adrenal glands from mice treated with $H_2O$ (vehicle, n=6) or antibiotic cocktail (ABX, n=7). (**F**) Immunostaining and confocal imaging of synaptophysin (green) and CHGA (red) in primary cultured chromaffin cells from WT and *Lyz1*$^{-/-}$ mice (treated with iE-DAP or PBS). Scale bars, 10 μm (**A**, **F**); 50 μm (**C**). Statistically significant differences were determined using the Mann-Whitney test (**D**, **E**). \*\**p*<0.01 and

29

808    ****$p<0.0001$. Each symbol represents an individual mouse. Mean and s.e.m. are indicated (**D**, **E**).

809    Data (**A**-**F**) are representative of three independent experiments.
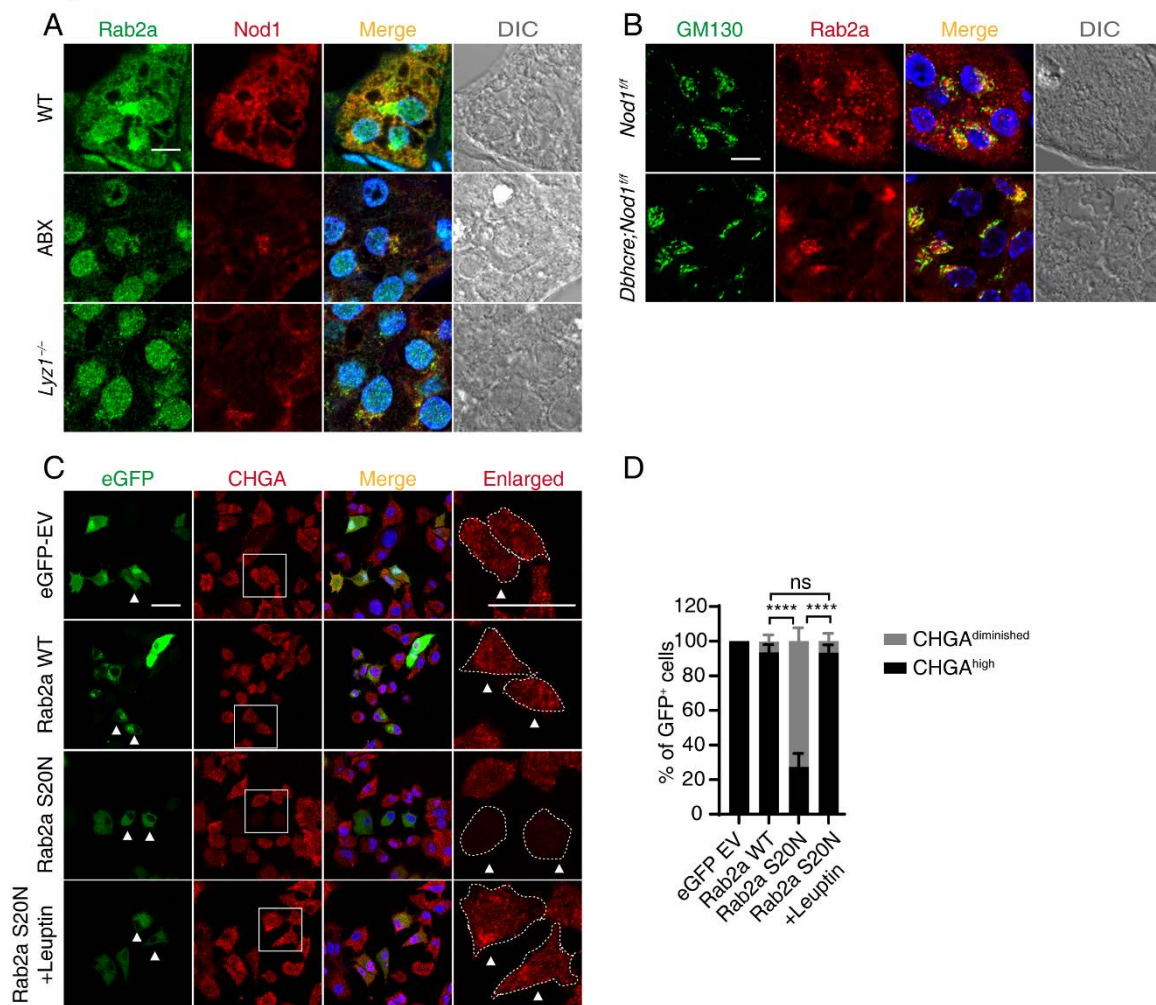
**Figure 3.** Nod1 recruits Rab2a onto DCGs to regulate CHGA retention in DCGs. (**A**) Immunostaining and confocal imaging of Rab2a (green) and Nod1 (red) in paraffin sections of adrenal gland from WT, ABX and *Lyz1⁻/⁻* mice. (**B**) Immunostaining and confocal imaging of GM130 (green) and Rab2a (red) in paraffin sections of adrenal gland from *Nod1^{f/f}* and *Dbh-cre;Nod1^{f/f}* mice. (**C**) PC-12 cells were transfected with eGFP empty vector (EV), wild-type Rab2a tagged with eGFP, or a dominant-negative Rab2a-S20N mutant tagged with eGFP. Cells were immunostained with anti-CHGA (red) antibody. Cells in the boxed regions are highly magnified on the right. White dashed line outlines the designated cell boundry. Arrowheads indicate representative GFP⁺ cells. (**D**) Quantification of transfected (GFP⁺) CHGA^diminished cells and CHGA^high cells from (**C**). Cells were counted from 8-10 fields of view with at least 140 GFP⁺ cells quantified for each sample. Scale bars, 10 μm in (**A**, **B**), 30 μm in (**C**). Statistically significant differences were determined using one-way ANOVA followed by Tukey's post hoc tests (**D**). ****$p<0.0001$. ns indicates no significant

822    difference. Summary plot shows means and s.e.m. (**D**). Data (**A**-**D**) are representative of three
823    independent experiments.

**Figure 4**
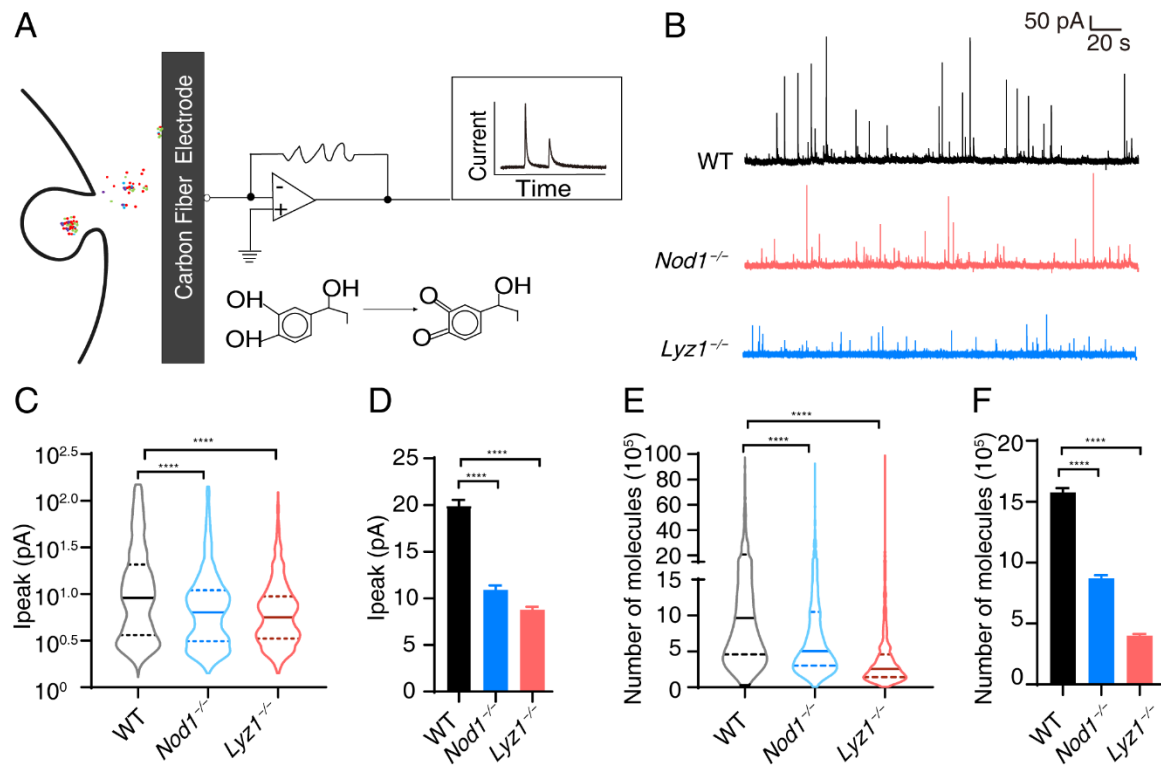


824    **Figure 4.** Amperometry recordings reveal a significant decrease in the number of catecholamine
825    molecules released by individual vesicles in *Nod1*$^{-/-}$ and *Lyz1*$^{-/-}$ adrenal chromaffin cells. (**A**)
826    Schematic diagram of the amperometry recording experiment. (**B**) Representative amperometric
827    traces from WT, *Nod1*$^{-/-}$ and *Lyz1*$^{-/-}$ chromaffin cells. (**C**) Violin plot of peak current of each
828    amperometric spike event from WT (n=2031 events), *Nod1*$^{-/-}$ (n=1243 events) and *Lyz1*$^{-/-}$ (n=1317
829    events) chromaffin cells. (**D**) Means of peak current from (**C**) were plotted with s.e.m. (**E**) Violin plot
830    of number of molecules in each amperometric spike event from WT (n=2172 events), *Nod1*$^{-/-}$
831    (n=1329 events) and *Lyz1*$^{-/-}$ (n=1341 events) chromaffin cells. (**F**) Means of number of molecules
832    from (**E**) were plotted with s.e.m. Statistically significant differences were determined using one-
833    way ANOVA followed by Tukey's post hoc tests (**C**-**F**). \*\**p*<0.01.
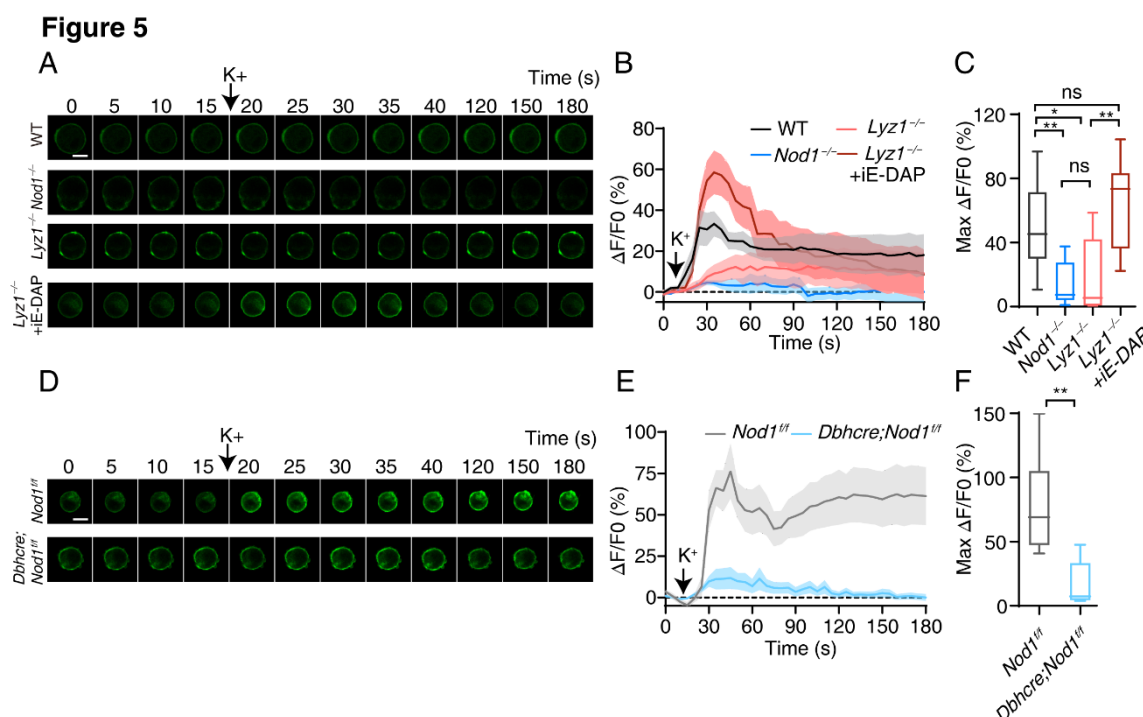
**Figure 5.** Reduced catecholamine secretion in chromaffin cells deficient in Nod1 or Nod1 ligand. (**A**) Representative images of green fluorescence of GRAB$_{NE}$ in transfected chromaffin cells from WT, $Nod1^{-/-}$ and $Lyz1^{-/-}$ (pretreated with iE-DAP for 6 h or PBS) during the course of treatment with $K^+$ solution (90 mM) to trigger secretion. (**B**) The recorded fluorescence changes of GRAB$_{NE}$ over the time course of the experiment ($\Delta F/F0$) (n=8-12 cells from 5-8 mice). (**C**) Box plot of the maximum peak of $\Delta F/F0$ from (**B**) with median and interquartile range indicated. (**D**) Representative images of green fluorescence of GRAB$_{NE}$ in transfected chromaffin cells from $Nod1^{f/f}$ and $Dbh$-$cre;Nod1^{f/f}$ mice during the course of treatment with $K^+$ solution (90 mM). (**E**) The recorded fluorescence changes of GRAB$_{NE}$ over the time course of the expriment ($\Delta F/F0$) (n=6-10 cells from 5-8 mice). (**F**) Box plot of the maximum peak of $\Delta F/F0$ from (**E**). The line connects means of fluorescence changes over the time course with ribbons indicating ± s.e.m. (**B**, **E**). Scale bars, 10 μm (**A**, **D**). Statistically significant differences were determined using one-way ANOVA followed by Tukey's post hoc tests (**C**) and Student's $t$-test (**F**). $*p<0.05$ $**p<0.01$, $***p<0.001$ and $****p<0.0001$.

33
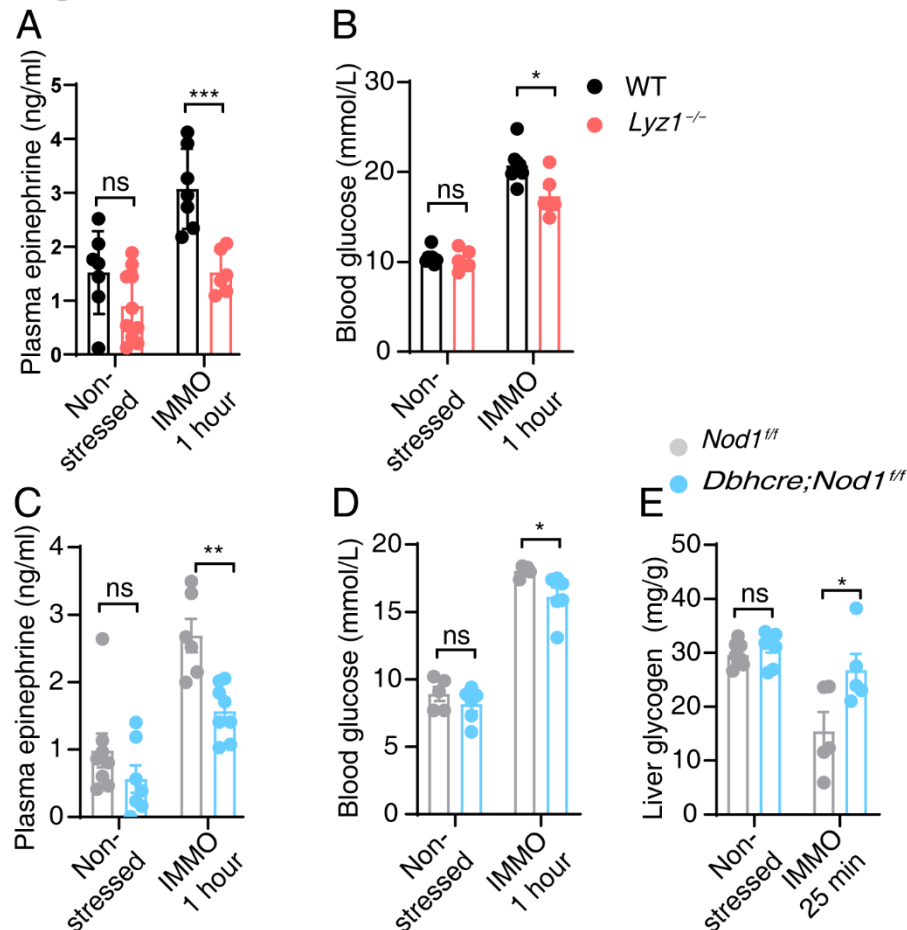
## Figure 6



847 **Figure 6.** Deficiency of Nod1 ligand impairs epinephrine response. Deficiency of Nod1 ligand

848 impairs epinephrine response. (**A**, **C**) Plasma level of epinephrine in the steady state and following

849 stress induction by immobilization (IMMO; 1 h) in WT, *Lyz1⁻ᐟ⁻*, *Nod1ᶠ/ᶠ* and *Dbh-cre;Nod1ᶠ/ᶠ* mice. (**B**,

850 **D**) Concentration of blood glucose in the steady state and following immobilization (IMMO; 1 h) in

851 WT, *Lyz1⁻ᐟ⁻*, *Nod1ᶠ/ᶠ* and *Dbh-cre;Nod1ᶠ/ᶠ* mice. (**E**) Liver glycogen content under steady-state

852 conditions or after 25 min IMMO in *Nod1ᶠ/ᶠ* and *Dbh-cre;Nod1ᶠ/ᶠ* mice. Statistically significant

853 differences were determined using one-way ANOVA followed by Tukey's post hoc tests (**A**-**E**). ns,

854 indicates no significant difference ($p>0.05$). *$p<0.05$, **$p<0.01$ and ***$p<0.001$. Summary plots (**A**-

855 **E**) show mean with s.e.m. Each symbol represents an individual mouse.

1  **Supplementary Information for**


2  **Intestinal microbiota modulates adrenomedullary response through Nod1 sensing in**
3  **chromaffin cells**

4  Chen Xiang[1, 2, #], Peihua Chen[3, #], Qin Zhang[1], Yinghui Li[1, 2], Ying Pan[1], Wenchun Xie[1, 4], Jianyuan

5  Sun [3, *], Zhihua Liu [1, 5, 6, *]

6  1. Key Laboratory of Infection and Immunity, Institute of Biophysics, Chinese Academy of Sciences,

7  Beijing 100101, China

8  2. University of Chinese Academy of Sciences, Beijing 100049, China

9  3. The Brain Cognition and Brain Disease Institute, Shenzhen Institutes of Advanced Technology,

10  CAS; Shenzhen-Hong Kong Institute of Brain Science-Shenzhen Fundamental Research

11  Institutions, Shenzhen, 518055, China

12  4. Guangdong Bio-healhtech Advanced Co., Ltd., Foshan 528000, China

13  5. Institute of Immunology, School of Medicine, Tsinghua University

14  6. Tsinghua-Peking Center for Life Sciences, 100084

15  #These authors contributed equally: Chen Xiang and Peihua Chen

16  *Corresponding authors

17  To whom correspondence may be addressed. Email: zhihualiu@ibp.ac.cn. or jy.sun1@siat.ac.cn.

18  ORCIDs: 0000-0002-0269-0901 Zhihua Liu; 0000-0002-1072-6230 Chen Xiang
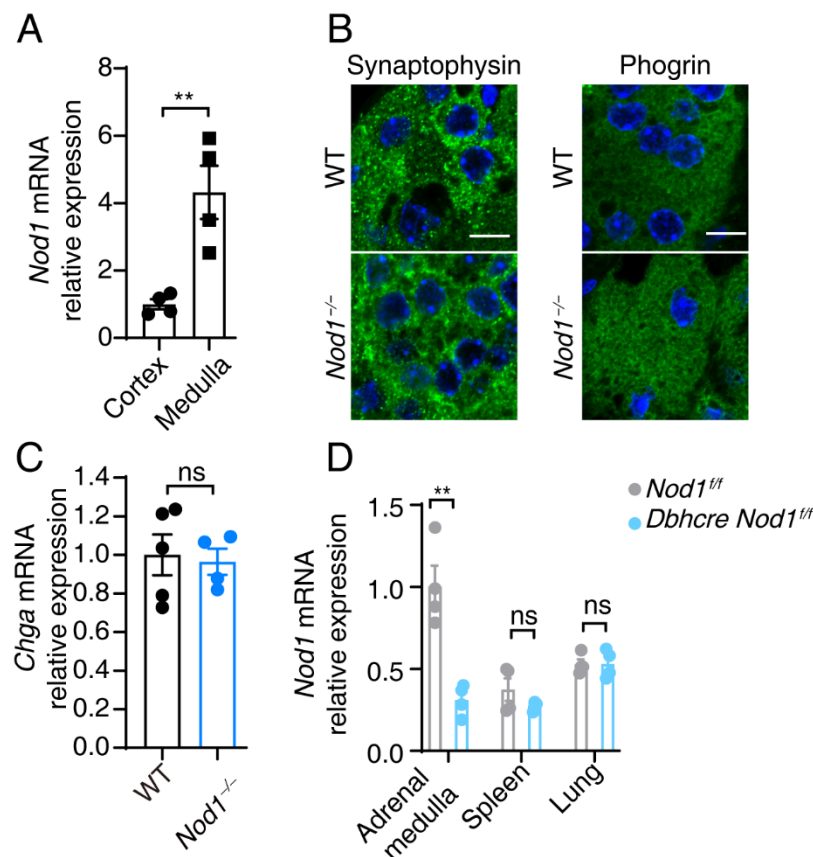
19  **This PDF file includes:**


20  **Figure 1—figure supplement 1**
21  **Figure 2—figure supplement 1**
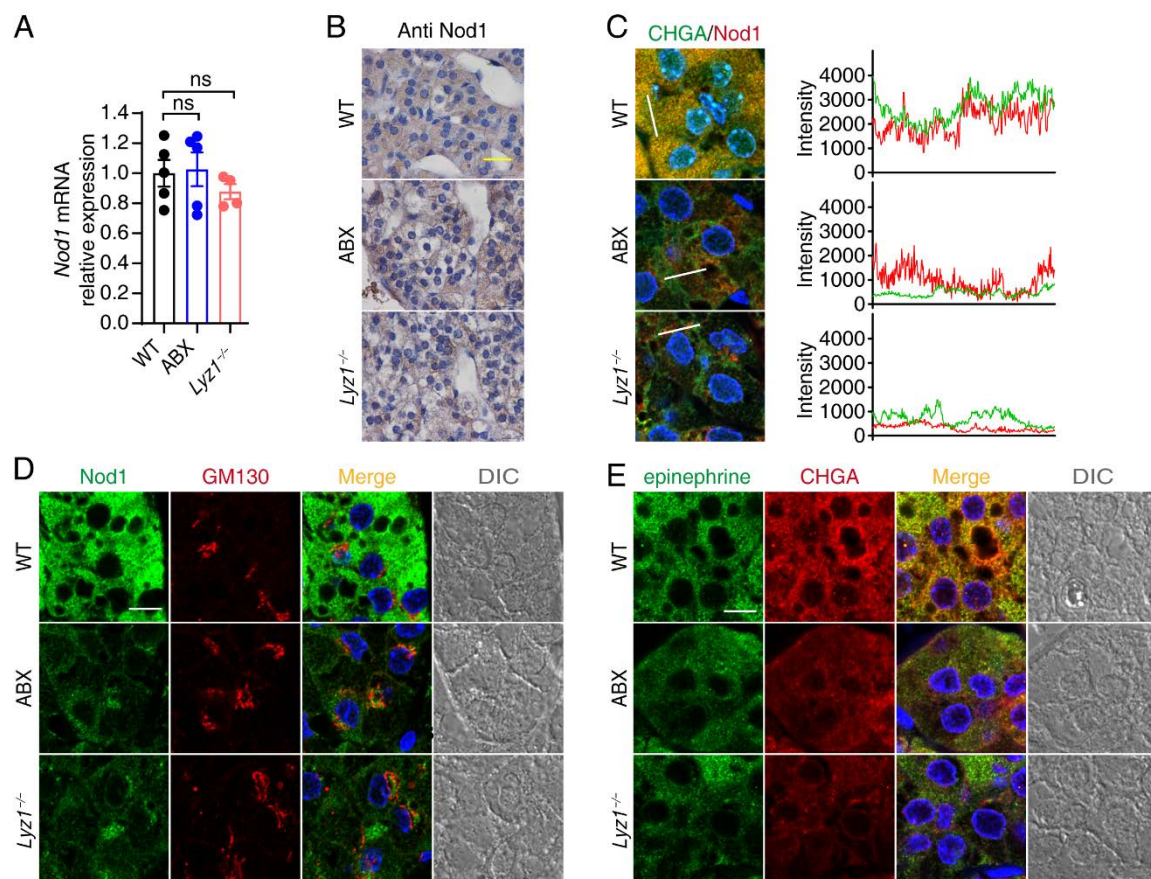22  **Figure 5—figure supplement 1**
23  **Materials**

# Figure 1—figure supplement 1



**Figure 1—figure supplement 1.** Nod1 is highly expressed in adrenal medulla. (**A**) Relative *Nod1* mRNA in adrenal medulla and adrenal cortex determined by qPCR. The *GAPDH* mRNA level was used for normalization. (**B**) Immunostaining and confocal imaging of synaptophysin and phogrin in paraffin sections of adrenal gland from WT and *Nod1$^{-/-}$* mice. (**C**) Relative *CHGA* mRNA level in adrenal medulla determined by qPCR. The *GAPDH* mRNA level was used for normalization. (**D**) Relative *CHGA* mRNA in adrenal medulla, spleen and lung of *Nod1*$^{f/f}$ and *Dbh-cre;Nod1*$^{f/f}$ mice determined by qPCR. The *GAPDH* mRNA level was used for normalization. Statistically significant differences were determined using Student's *t*-test (**A**, **C**), and ANOVA (**B**). ns, indicates no significant difference ($p$>0.05). \*\*$p$<0.01. Summary plots show mean with s.e.m. Each symbol represents the value from an individual animal.

**Figure 2—figure supplement 1**



**Figure 2—figure supplement 1.** Nod1 localizes on DCGs to direct CHGA retention. (**A**) Relative *Nod1* mRNA level in adrenal medulla from WT, ABX and *Lyz1⁻/⁻* mice. (**B**) Immunohistochemical staining (IHC) of Nod1 in paraffin sections of adrenal glands from WT, ABX and *Lyz1⁻/⁻* mice. (**C**) The RGB profiler plugin from ImageJ was used to plot colocalization of CHGA and Nod1 along the white lines drawn in the images, which correspond to the "Merge" images in Figure 2A. (**D**) Immunostaining and confocal imaging of Nod1 (green) and GM130 (red) in paraffin sections of adrenal gland from WT, ABX and *Lyz1⁻/⁻* mice. (**E**) Immunostaining and confocal imaging of epinephrine (green) and CHGA (red) in paraffin sections of adrenal gland from WT, ABX and *Lyz1⁻/⁻* mice. Statistically significant differences were determined using ANOVA (*A*). ns, indicates no significant difference ($p > 0.05$). Each symbol represents an individual mouse. Mean and s.e.m. are indicated.

3

**Figure 5—figure supplement 1**
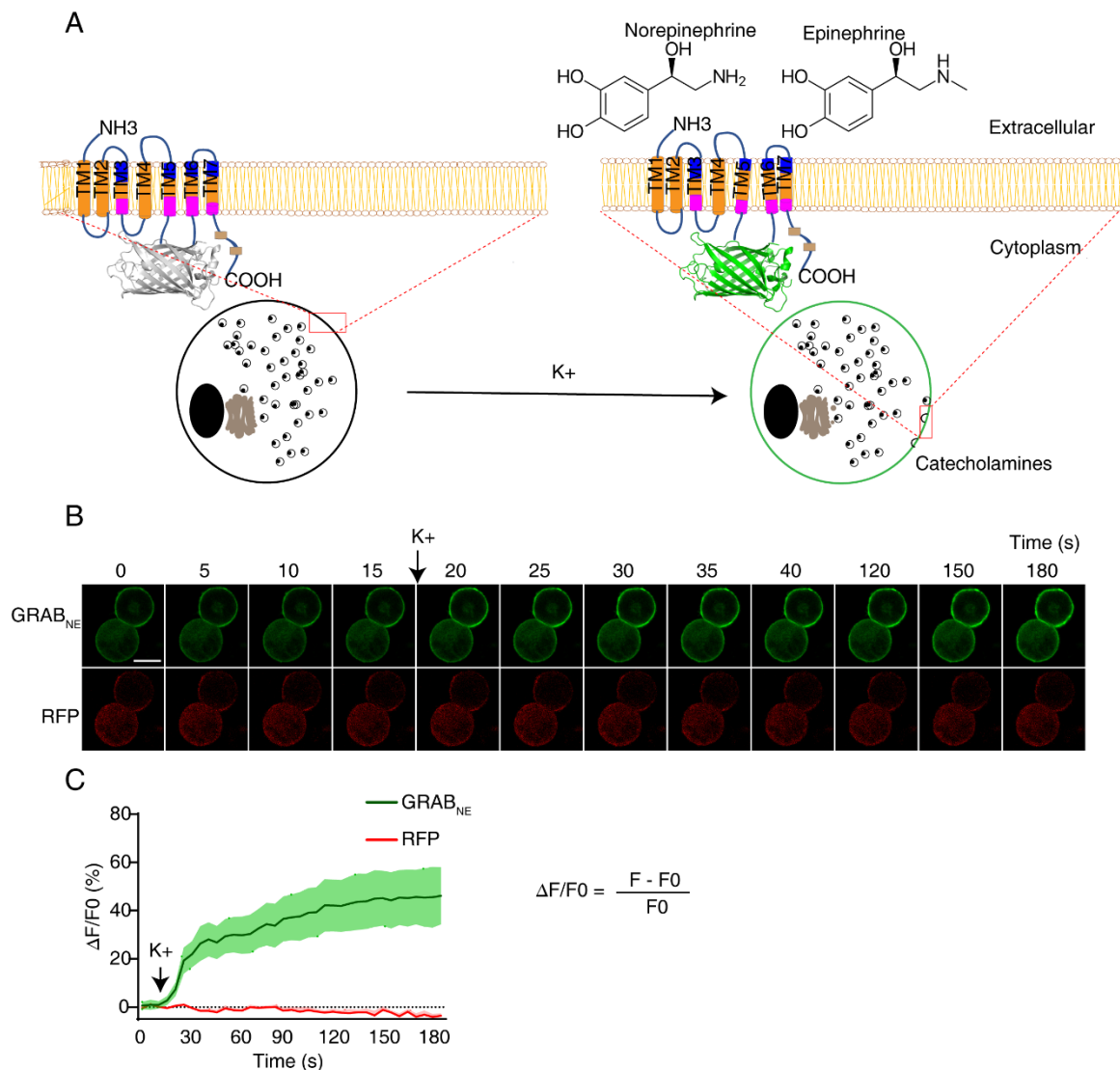


**Figure 5—figure supplement 1.** Epinephrine (norepinephrine) assay with GRABNE. (**A**) Schematic diagram of the *ex vivo* K+-stimulated catecholamine secretion assay. (**B**) Representative images of green fluorescence of GRABNE and red fluorescence of RFP in transfected chromaffin cells during the course of treatment. (**C**) The recorded fluorescence changes ($\Delta F/F0$) of GRABNE and RFP over the time course of the experiment (n= 5 cells from 3 mice). Scale bars,10 μm.

4

51  **Materials**

| Antibodies | Source | Identifier |
|---|---|---|
| Anti-Nod1 (IF, IHC) | Novus Biologicals | Cat# NB100-56878 |
| Anti-GM130 (IF) | BD Biosciences | Cat# 610822 |
| Anti-Rab2a | Proteintech | Cat# 15420-1-AP |
| Anti-Rab2a | Zen BioScience | Cat# 200506 |
| Anti-TGN38 | BD Biosciences | Cat# 610899 |
| Anti-synaptophysin | Thermo scientific | Cat# PA1-1043 |
| Anti-CHGA | Novus Biologicals | Cat# NBP2-4476 |
| Anti-CHGA | Abcam | Cat# ab15160 |
| Anti-TH | Novus Biologicals | Cat# NB300-110 |
| Anti-GAPDH | Immunoway | Cat# YT5052 |
| Anti-beta actin | ZSGB-BIO | Cat# TA-09 |
| Anti-Epinephrine | Abbexa | Cat# ABX100507 |
| Goat anti-Rabbit IgG (H+L) Cross-Adsorbed Secondary Antibody, Alexa Fluor 555 | Thermo Fisher | Cat# A21428 |
| Goat anti-mouse IgG (H+L) Cross-Adsorbed Secondary Antibody, Alexa Fluor 555 | Thermo Fisher | Cat# A21422 |
| Goat anti-Rabbit IgG (H+L) Cross-Adsorbed Secondary Antibody, Alexa Fluor 488 | Thermo Fisher | Cat# A11008 |
| Goat anti-mouse IgG (H+L) Cross-Adsorbed Secondary Antibody, Alexa Fluor 488 | Thermo Fisher | Cat# A11001 |
| Goat anti-Rat IgG (H+L) Cross-Adsorbed Secondary Antibody, Alexa Fluor 488 | Thermo Fisher | Cat# A11006 |
| Donkey anti-sheep IgG (H+L) Cross-Adsorbed Secondary Antibody, Alexa Fluor 594 | Invitrogen | Cat# A11016 |
| Donkey anti-mouse IgG (H+L) Cross-Adsorbed Secondary Antibody, Alexa Fluor 488 | Proteintech | Cat# SA00013-5 |

| Goat anti-Mouse IgG (H+L) pAb-HRP | MBL | Cat# 330 |
| Mouse anti-Rabbit IgG-HRP | Southern Biotech | Cat# 4090-05 |

| **Reagents** | **Source** | **Identifier** |
| --- | --- | --- |
| Normal goat serum blocking reagent | Boster Biotech | Cat# AR1009 |
| DAPI | Novon | Cat# SS0156 |
| Fluoromount-G | Southern Biotech | Cat# 0100-01 |
| DAB Peroxidase (HRP) substrate | Maixin Biotech | Cat# DAB-0031 |
| Hematoxylin solution | Sigma-Aldrich | Cat# 03971 |
| PageRuler Prestained protein Ladder | Thermo Fisher | Cat# 26616 |
| Pure nitrocellulose blotting membrane | PALL | Cat# P/N 66485 |
| Luminata Forte Western | Millipore | Cat# WBLUF0100 |
| DMEM | Hyclone | Cat# sh3002201B |
| FBS | Bioind | Cat# 04-001-1A |
| RPMI 1640 Medium | Gibco | Cat# 11875-093 |
| Endotoxin free PBS | Gibco | Cat# 10010-023 |
| Lipofectamine 2000 | Thermo Fisher | Cat# 11668019 |
| Hexadimethrine bromide (polybrene) | Sigma-Aldrich | Cat# H9268 |
| Trizol | Thermo Fisher | Cat# 15596018 |
| iE-DAP | InvivoGen | Cat# tlrl-dap |
| PrimeScript RT reagent Kit | TAKARA | Cat# DRR047A |
| SYRB Premix Ex Taq | TAKARA | Cat# DRR820A |
| Adrenaline Research ELISA | Labor Diagnostika Nord | Cat# BA E-5100 |

| UltraSensitive TM S-P Kit mouse | Maixin Biotech | Cat# KIT-9701 |
| --- | --- | --- |
| UltraSensitive TM S-P Kit rabbit | Maixin Biotech | Cat# KIT-9706 |
| Leupeptin | Leagene Biotechnology | Cat# PI0029 |
| **Recombinant DNA** | **Source** | **Identifier** |
| pDisplay-NE1m-IRES-mCherry-CAAX | (*Feng et al., 2019*) | N/A |
| peGFP-C1 | Addgene | Cat# 6084-1 |
| Rab2a cDNA cloned from HEK-293T | This study | N/A |
| **Cell lines** | **Source** | **Identifier** |
| PC-12 | China Infrastructure of Cell Line Resources | Cat# TCR 8 |
| **Strains** | **Source** | **Identifier** |
| Mouse: *Nod1* $^{-/-}$ | Our lab (*Zhang et al., 2019*) | N/A |
| Mouse: *Lyz1* $^{-/-}$ | Our lab (*Zhang et al., 2019*) | N/A |
| Mouse: *Dbh Cre* | MMRRC | RRID: MMRRC_036734-UCD |
| Mouse: *Nod1$^{f/f}$* | Our lab (*Zhang et al., 2019*) | N/A |
| Mouse: C57BL/6J | C57BL/6JTshu | N/A |
| **Software and Algorithms** | **Source** | **Identifier** |
| GraphPad Prism v8 | GraphPad software | https://www.graphpad.com/scientificsoftware/prism |
| Image J v1.48 | NIH | https://imagej.nih.gov/ij/ |
| Zeiss Zen Imaging software (blue edition) | Zeiss | https://www.zeiss.com/microscopy/int/softwarecameras.html |
| Nikon-Elements Advanced Research | Nikon | www.microscope.healthcare.nikon.com |
| **qPCR primers** | 5'-3' | |

| | |
|---|---|
| Nod1-F (mouse) | GGTCACCAACATTCGGAACA |
| Nod1-R (mouse) | CTTTCGGACCTTGTCAGGC |
| Chga-F (mouse) | GCTCCAAGACCTCGCTCTCC |
| Chga-R (mouse) | CCTGATTGTTCCCCTCAGCCT |
| Gapdh-F (mouse) | TGTTCCTACCCCCAATGTGT |
| Gapdh-R (mouse) | GGTCCTCAGTGTAGCCCAAG |

52 **References、**

53 Feng, J., Zhang, C., Lischinsky, J. E., Jing, M., Zhou, J., Wang, H., . . . Li, Y. (2019). A Genetically
54    Encoded Fluorescent Sensor for Rapid and Specific In Vivo Detection of Norepinephrine. *Neuron,*
55    *102*(4), 745-761.e748. doi:10.1016/j.neuron.2019.02.037
56 Zhang, Q., Pan, Y., Zeng, B., Zheng, X., Wang, H., Shen, X., . . . Liu, Z. (2019). Intestinal lysozyme
57    liberates Nod1 ligands from microbes to direct insulin trafficking in pancreatic beta cells. *Cell Res,*
58    *29*(7), 516-532. doi:10.1038/s41422-019-0190-3